Constraints on squark and gluino masses in R-parity violating scenarios from jet triplet resonance searches

Håvard Sannes

Master's thesis
June 1, 2012
Department of Physics
University of Oslo

Abstract

This thesis begins with the formulation of supersymmetry. Further on, the concept of R-parity is introduced, squarks and gluinos that can interact through R-parity violating couplings are studied, bounds on their masses at 95 % confidence level are found by use of Monte Carlo simulations for proton–proton collisions at 7 TeV.

Acknowledgements

First I would like to thank my advisor Are Raklev who has been very helpful, encouraging and patient. I would also like to thank my fellow students Veronica, Lars, Anders, Ola and Paul for discussions related to my thesis. Thanks to Bjørn Aage and Nadia who have been helping with the grammar. Finally I want to thank my family for their moral support.

Contents

Chapter 1

Introduction

There are a certain number of problems in particle physics today that the Standard Model (SM) fails to explain; there are no Standard Model candidates for dark matter, the origin of the Higgs potential is unknown, and in order to explain the assumed mass of the Higgs boson one needs an extreme fine tuning.

There has been proposed a number of theories which at some level explain one or several of these problems. One theory that by many physicists is regarded to all of solve these problems is supersymmetry (SUSY), a symmetry that relates elementary particles of a given spin to other elementary particles with a spin that differs by one half. It turns out that supersymmetry is not a symmetry between different particles in the Standard Model , so one has to introduce additional particles (superpartners of Standard Model particles), and these are yet to be discovered.

Originally, it was thought that Supersymmetry was an unbroken theory, this is that for every fermion there should be a boson with the same quantum numbers except for spin. Throughout the last decades a lot of effort has been spent to find these particles, but there has been no hint of their appearance in the mass region where the standard model particles exist. Therefore one has been forced to give up the idea of an unbroken theory, the difference in mass cannot even be explained by a spontaneously broken theory at low scales, so instead one introduces an explicit symmetry breaking, which gives rise to a splitting between the Standard Model particles and their superpartners. This leads to a lot of free parameters. The manifestation of SUSY is introduced at the TeV scale, as this can explain both the behaviour of dark matter and the order of the Higgs mass.

The Standard Model can be extended to involve the superpartners of the Standard Model particles and their interactions as well. It turns out that some of the terms that appear in this generalized Lagrangian breaks the so called R-parity symmetry, this means that either baryon number and/or lepton number conservation is broken too. One of the main consequences, at a first glance, is that R-parity violation would lead to proton decay, which is the most important motivation for

imposing R-parity conservation. However, it turns out that the stability of the proton can be ensured in other ways.

In this thesis I will discuss my study of the superpartners of quarks (squarks) and gluons (gluinos) in R-parity violating (RPV) models. I have performed a numerical study involving production of squarks and gluinos from proton-proton collisions at 7 TeV, with decay through a R-Parity violating coupling. The resulting jets have been studied, and from results published by the CMS experiment [1] I have been able to set bounds on squark and gluino masses at 95% confidence level. I begin in Chapter 2 by discussing the formulation of SUSY and its consequenses. Chapter 3 describes the numerical study of squarks and gluinos. Chapter 4 is concerned with a radiation process that is treated inaccurately in the numerical simulation. Finally concluding remarks are contained in Chapter 5.

Chapter 2

Supersymmetry

In this chapter the foundations of Supersymmetry and its consequences are discussed. It has been shown that Supersymmetry is the largest possible space-time extension of the Lorentz symmetry [2]. This section is based on *A Supersymmetry primer* by Martin [3], the review paper on R-parity violating supersymmetry by Barbier *et al.* [4], and the lecture notes from the course Fys 5120 lectured at the University of oslo.

2.1 The origin of SUSY

2.1.1 The Super-Poincaré algebra

In special-relativity the boosts and translations are described by the Poincaré group.

$$x'^{\mu} = \Lambda^{\mu}_{\nu} x^{\nu} + a^{\mu} \tag{2.1}$$

where x^{μ} is a coordinate four-vector, Λ^{μ}_{ν} is the Lorentz boost and a^{μ} is a translation parameter. The translation is generated by the operator P_{μ}. Lorentz boosts and rotations are generated by the operator $M_{\mu\nu}$. These operators form the Poincaré algebra

$$[P_{\mu}, P_{\nu}] = 0 \tag{2.2}$$
$$[M_{\mu\nu}, M_{\rho\sigma}] = -i\left(g_{\mu\rho}M_{\nu\sigma} - g_{\mu\sigma}M_{\nu\rho} - g_{\nu\rho}M_{\mu\sigma} + g_{\nu\sigma}M_{\mu\rho}\right) \tag{2.3}$$
$$[M_{\mu\nu}, P_{\rho}] = -i\left(g_{\mu\rho}P_{\nu} - g_{\nu\rho}P_{\mu}\right) \tag{2.4}$$

which is a Lie algebra. A Lie algebra is an algebra where the the binary operator $[,]$ has the following three properties for x, y, $z \in L$.

$$[ax + by, z] = a[x, z] + b[y, z], \tag{2.5}$$
$$[x, y] = -[y, x], \tag{2.6}$$
$$[x, [y, z]] + [y, [z, x]] + [z, [x, y]] = 0, \tag{2.7}$$

In 1967 Coleman and Mandula [5] proved that it's not possible to extend the space-time symmetries described by the Poincaré group using Lie-algebra in a non-trivial way. However, in 1975 Haag, Lopuszanski and Sohnius [2] showed that this indeed can be done be defining a new type of algebra called a graded Lie algebra, which is defined as follows. The graded Lie algebra or superalgebra is a vector space L that is a direct sum of two vector spaces L_0 and L_1 with a binary operation that has the following properties:

$$x_i * x_j \in L_{(i+j)\mathrm{mod}_2}, \tag{2.8}$$
$$x_i * x_j = -(-1)^{ij} x_j * x_i, \tag{2.9}$$
$$x_i * (x_j * x_k)(-1)^{ik} + x_j * (x_k * x_i)(-1)^{ji} = -x_k * (x_i * x_j)(-1)^{kj}. \tag{2.10}$$

In order to get a set of generators that are compatible with this algebra one introduces the operator Q_a. This operator acts on spins-states, it transforms fermionic states into bosonic states and vice versa. It can be written in terms of left and right Weyl spinors Q_A and $Q^{\dot{A}}$.

$$Q_a = \begin{pmatrix} Q_A \\ Q^{\dot{A}} \end{pmatrix}. \tag{2.11}$$

In addition to the relations in the Poincaré algebra the super-Poincaré algebra is defined by these relations

$$\{Q_A, Q_B\} = 0, \tag{2.12}$$
$$\{Q_{\dot{A}}, Q_{\dot{B}}\} = 0, \tag{2.13}$$
$$\{Q_A, Q_{\dot{B}}\} = 2\sigma^{\mu}_{A\dot{B}} P_\mu, \tag{2.14}$$
$$[Q_A, P_\mu] = 0, \tag{2.15}$$
$$[Q_{\dot{A}}, P_\mu] = 0, \tag{2.16}$$
$$[Q_A, M_{\mu\nu}] = i\sigma_A^{\mu\nu B} Q_B. \tag{2.17}$$

Here $\sigma^{\mu\nu} = \sigma^\mu \bar{\sigma}^\nu - \sigma^\nu \bar{\sigma}^\mu$. Here $\sigma^\mu = (1, \vec{\sigma})$ and $\bar{\sigma^\mu} = (1, -\vec{\sigma})$, where $\vec{\sigma}$ is a vector of the three Pauli matrices defined in the Appendix B. The relations above are those of $N = 1$ supersymmetry. A $N > 1$ supersymmetry introduces supermultiplets of Q operators and particles. I will only consider $N = 1$ supersymmetry in this thesis.

2.1.2 Superspace

Superspace is an eight-dimensional manifold that can be constructed from the coset space of the Super-Poincaré group SP and the Lorentz group L, SP/L. The superspace coordinates are given by

$$z^{\pi} = \left(x^{\mu}, \theta^{A}, \bar{\theta}^{\dot{A}}\right). \tag{2.18}$$

An element g in the Super-Poincaré group can be written.

$$g = \exp[-ix^{\mu}P_{\mu} + i\theta^{A}Q_{A} + i\bar{\theta}_{\dot{A}}Q^{\dot{A}} - \frac{i}{2}\omega_{\rho\nu}M^{\rho\nu}]. \tag{2.19}$$

An element $g_0 \in SP/L$ can be written in the following way [6]

$$L\left(x,\theta\right) = \exp[-ix^{\mu}P_{\mu} + i\theta^{A}Q_{A} + i\bar{\theta}_{\dot{A}}Q^{\dot{A}}]. \tag{2.20}$$

The θ coordinates are Grassman numbers and the coordinates of superspace satisfy these relations:

$$[x^{\mu}, x^{\nu}] = [x^{\mu}, \theta^{A}] = [x^{\mu}, \theta^{\dot{A}}] = 0 \tag{2.21}$$

$$\{\theta^{A}, \theta^{B}\} = \{\theta^{A}, \theta^{\dot{B}}\} = \{\theta^{\dot{A}}, \theta^{B}\} = \{\theta^{\dot{A}}, \theta^{\dot{B}}\} = 0 \tag{2.22}$$

The integral is defined over Grassman variables as

$$\int d\theta_{A} = 0, \tag{2.23}$$

$$\int d\theta_{A}\theta_{A} = 1. \tag{2.24}$$

The four-Grassman number integral is the one that is used the most, and its most important property is

$$\int d\theta^{4}\theta^{2}\bar{\theta}^{2} = 1. \tag{2.25}$$

An element $g_0 \in SP/L$ acts on superspace coordinate z^{π} with the mapping

$$g_0 e^{iz^{\pi}K_{\pi}} = e^{iz'^{\pi}K_{\pi}}, \tag{2.26}$$

were the generators of the group SP/L are K_{π}

$$K_{\pi} = \left(P_{\nu}, Q_{B}, Q^{\dot{B}}\right). \tag{2.27}$$

By explicit calculation one finds that

$$g_0 e^{iz^\pi K_\pi} = \exp\left[i\left(-x^\mu - a^\mu + i\alpha^\mu\sigma^\mu_{A\dot{A}}\bar{\theta}^{\dot{A}} - i\theta\sigma^\mu_{A\dot{A}}\bar{\alpha}^{\dot{A}}\right)P_\mu \right. \\ \left. + i\left(\theta^A + \alpha^A\right)Q_A + i\left(\bar{\theta}^{\dot{A}} + \bar{\alpha}^{\dot{A}}\right)Q_{\dot{A}}\right]. \tag{2.28}$$

Which leads to

$$\left(x^\mu, \theta^A, \bar{\theta}^{\dot{A}}\right) \to f_i\left(a^\mu, \alpha^A, \bar{\alpha}_{\dot{A}}\right) = \\ \left(x^\mu + a^\mu - i\alpha^A\sigma^\mu_{A\dot{A}}\bar{\theta}^{\dot{A}} + i\theta^A\sigma^\mu_{A\dot{A}}\bar{\alpha}^{\dot{A}}, \theta^A + \alpha^A, \bar{\theta}_{\dot{A}} + \bar{\alpha}_{\dot{A}}\right) \tag{2.29}$$

when comparing both sides of Eq. (2.26).

The differential representation of generators at a Lie group are given by

$$x_j = \frac{\partial f_i}{\partial a_j}\frac{\partial}{\partial x_i}. \tag{2.30}$$

This gives an explicit differential representation for the generators

$$P_\mu = i\partial_\mu \tag{2.31}$$
$$iQ_A = -i\left(\sigma^\mu\bar{\theta}\right)_A\partial_\mu + \partial_A \tag{2.32}$$
$$i\bar{Q}^{\dot{A}} = -i\left(\bar{\sigma}^\mu\theta\right)^{\dot{A}}\partial_\mu + \partial^{\dot{A}}. \tag{2.33}$$

This further motivates for defining the covariant derivative in a SUSY invariant way

$$D_A = i\left(\sigma^\mu\bar{\theta}\right)_A\partial_\mu + \partial_A \tag{2.34}$$
$$\bar{D}_{\dot{A}} = -i\left(\sigma^\mu\theta\right)_{\dot{A}}\partial_\mu - \partial_{\dot{A}}. \tag{2.35}$$

2.1.3 Superfields

A superfield is a function structure defined on superspace that contains various component fields, these fields could be fields of fermions, scalars or vector bosons. A general superfield can be written as

$$\Phi\left(x, \theta, \bar{\theta}\right) = f(x) + \theta^A\varphi_A(x) + \bar{\theta}_{\dot{A}}\chi^{\dot{A}}(x) + \theta^2 m(x) + \bar{\theta}^2 n(x) \\ + \theta\sigma^\mu\bar{\theta}V_\mu(x) + \theta^2\bar{\theta}_{\dot{A}}\lambda^{\dot{A}}(x) + \bar{\theta}^2\theta^A\psi_A(x) + \theta^2\bar{\theta}^2 d(x). \tag{2.36}$$

Here

$$\theta^2 = \theta_A\theta^A \tag{2.37}$$

Component field	Type	d.o.f
$f(x), m(x), n(x)$	complex pseudo scalar	2
$\psi_A(x), \varphi_A(x)$	left handed Weyl spinors	4
$\bar{\chi}^{\dot{A}}(x), \bar{\lambda}^{\dot{A}}(x)$	right handed Weyl spinors	4
$V_\mu(x)$	lorentz4-vector	8
$d(x)$	complex scalar	2

Table 2.1: Fields contained in a general superfield

and

$$\bar{\theta}^2 = \theta^{\dot{A}}\bar{\theta}_{\dot{A}}. \tag{2.38}$$

The properties of the component fields in the expression for the superfield are listed in Table 2.1

In further calculations 3 kinds of superfields will be important: Left handed superfields, defined by $\bar{D}_{\dot{A}}\Phi = 0$. Right handed superfields defined by $D_A\Phi^\dagger = 0$ and vector superfields defined by $\Phi = \Phi^\dagger$.

From the covariant derivative one can define the following projection operators:

$$\pi_+ \equiv -\frac{1}{16\Box}\bar{D}^2D^2, \tag{2.39}$$

$$\pi_- \equiv -\frac{1}{16\Box}D^2\bar{D}^2, \tag{2.40}$$

$$\pi_T \equiv \frac{1}{8\Box}\bar{D}^2_{\dot{A}}\bar{D}^{\dot{A}}. \tag{2.41}$$

Where the D'Alembert operator is given by

$$\Box = \partial^\mu\partial_\mu. \tag{2.42}$$

The operators π_+ and π_- project of the left handed and the right handed part of a superfield respectively, that is because:

$$\pi_+\left(\bar{D}_{\dot{A}}\Phi\right) = \pi_-\left(D_A\Phi^\dagger\right) = 0 \tag{2.43}$$

The operator $\pi_T = 1-(\pi_+ + \pi_-)$, the three projection operators fulfill the following relations

$$\pi^2_{\pm,T} = \pi_{\pm,T} \tag{2.44}$$

$$\pi_+\pi_- = 0 \tag{2.45}$$

$$\pi_+\pi_T = 0 \tag{2.46}$$

$$\pi_-\pi_T = 0. \tag{2.47}$$

In order to eliminate the $\bar{\theta}$ dependence in the left handed superfield one introduces the transformation:

$$y^{\mu} = x^{\mu} + i\theta\sigma^{\mu}\bar{\theta}. \tag{2.48}$$

This change in coordinate gives

$$D_A = 2i\sigma^{\mu}_{A\dot{A}}\bar{\theta}^{\dot{A}}\frac{\partial}{\partial y^{\mu}} + \partial_A \tag{2.49}$$

$$\bar{D}_{\dot{A}} = -\partial_{\dot{A}}. \tag{2.50}$$

Using the Eq. (2.50) and the fact that $\bar{D}_{\dot{A}}\Phi = 0$, one gets that the superfield as function of y cannot contain any $\bar{\theta}$ components and can therefore be written as

$$\Phi(y,\theta) = A(y) + \sqrt{2}\theta\psi(y) + \theta^2 F(y). \tag{2.51}$$

Properties of these fields are shown in Table 2.2. One can do the inverse transfor-

Component field	Type	d.o.f
$A(x), F(x)$	Complex scalar	2
$\psi(x)$	Left handed Weyl spinors	4

Table 2.2: Component fields contained in a left handed superfield

mation and obtain the expression for the superfield as a function of x.

$$\Phi\left(x,\theta,\bar{\theta}\right) = A(x) + i\left(\theta\sigma^{\mu}\bar{\theta}\right)\partial_{\mu}A(x) - \frac{1}{4}\theta^2\bar{\theta}^2\Box A(x) + \sqrt{2}\theta\psi(x) - \frac{i}{\sqrt{2}}\theta^2\partial_{\mu}\psi(x) + \theta^2 F(x) \tag{2.52}$$

Here A is a scalar field, ψ is a fermionic field and F is an auxiliary field. Auxiliary fields do also appear in vector fields, these fields will be called D. It can be shown that the auxiliary fields will not appear in kinetic terms in the Lagrangian, they can thus be eliminated by the use of the Euler-Lagrange equations [3]. This elimination results in new interactions, for instance the scalar four couplings originates from the elimination of auxiliary fields. The auxiliary fields also give rise to some of the terms in the Higgs potential from the Radiative ElectroWeak Symmetry Breaking (REWSB).

The same procedure can be carried out for the right handed superfield as was done for the left handed one.
A vector superfield can in general be written

$$\begin{aligned}\Phi\left(x,\theta,\bar{\theta}\right) = {} & f(x) + \theta\varphi(x) + \bar{\theta}\bar{\varphi}(x) + \theta^2 m(x) + \bar{\theta}^2 m^*(x) \\ & + \theta\sigma^{\mu}\bar{\theta}V_{\mu}(x) + \theta^2\bar{\theta}\bar{\lambda}(x) + \bar{\theta}^2\theta\lambda(x) + \theta^2\bar{\theta}^2 d(x).\end{aligned} \tag{2.53}$$

Component field	Type	d.o.f
$f(x), d(x)$	Real scalar field	1
$\varphi(x), \lambda(x)$	Weyl spinors	4
$m(x)$	Complex scalar field	2
$V_\mu(x)$	Lorentz 4-vector	4

Table 2.3: Component fields contained in a vector superfield

Some properties of these component fields are shown in Table 2.3.

The vector field describes vector bosons and superpartners of vector bosons, so the vector superfield should contain only one left handed spinor λ, one complex scalar ,and one real vector field V_μ. This can be fixed by introducing the so-called supergauge transformation of a vector superfield

$$V'\left(x,\theta,\bar{\theta}\right) = V\left(x,\theta,\bar{\theta}\right) + \Phi\left(x,\theta,\bar{\theta}\right) + \Phi^\dagger\left(x,\theta,\bar{\theta}\right), \tag{2.54}$$

where Φ is a left-handed superfield. This leads to concrete transformations of the component fields, by fixing these transformations in a specific one obtains the Wess-Zumino gauge for vector superfields

$$V_{WZ}\left(x,\theta,\bar{\theta}\right) = \left(\theta\sigma^\mu\bar{\theta}\right)\left[V_\mu(x) + i\partial_\mu\left(A(x) - A^*(x)\right)\right] + \theta^2\bar{\theta}\bar{\lambda}(x) + \bar{\theta}^2\theta\lambda(x) + \theta^2\bar{\theta}^2 D(x). \tag{2.55}$$

Here D is the auxiliary field that can be eliminated as mentioned earlier in this section.

2.2 Construction of a SUSY Lagrangian

One defines the SUSY action in the following way

$$S = \int d^4x \int d^4\theta \mathcal{L}. \tag{2.56}$$

One requires that the SUSY action S should be invariant under SUSY transformations by construction. Which is consistent with the fact that the highest order component fields in θ and $\bar{\theta}$ in the Lagrangian always transform as derivatives [6].

By demanding that our Lagrangian should give rise to a renormalizable theory, it can be shown that the Lagrangian cannot contain terms with more than three powers of scalar superfields ϕ [7]. It can also be shown that a SUSY Lagrangian that satisfies the constraints above must be written in the following way

$$\mathcal{L} = \Phi_i^\dagger \Phi_i + \bar{\theta}^2 W[\Phi] + \theta^2 W[\Phi^\dagger]. \tag{2.57}$$

The structure W is called the superpotential, the term with only one field in the superpotential is called the tadpole term, while the ones with two and three fields are called the mass term and Yukawa term respectively.

$$W[\Phi] = t_i\Phi_i + m_{ij}\Phi_i\Phi_j + \lambda_{ijk}\Phi_i\Phi_j\Phi_k \tag{2.58}$$

2.2.1 Gauge theories

The generators of a Lie group G involved in gauge theories are described by the Lie-algebra

$$[t_a, t_b] = if^c_{ab}t_c. \tag{2.59}$$

For an element $g \in G$ one can write out the unitary representation that transforms a field Ψ

$$\Psi' = U(g)\,\Psi. \tag{2.60}$$

The representation is given as an exponential map

$$\Psi' = e^{-i\alpha^a t_a}\Psi. \tag{2.61}$$

Here α is the parameter of the transformation. In order for SUSY to inherit this transformation from the SM one defines that the left handed superfield transforms as

$$\Psi' = e^{-iq\Lambda^a t_a}\Psi. \tag{2.62}$$

Here the transformation parameter Λ^a is a left handed superfield and q is the charge under G of Ψ. For the superpotential to be invariant one must then have the following identities

$$g_i = 0 \text{ if } g_i U_{ir} \neq g_r, \tag{2.63}$$
$$m_{ij} = 0 \text{ if } m_{ij}U_{ir}U_{js} \neq m_{rs}, \tag{2.64}$$
$$\lambda_{ijk} = 0 \text{ if } \lambda_{ijk}U_{ir}U_{js}U_{kt} \neq \lambda_{rst}. \tag{2.65}$$

In order for the kinetic term to be invariant under the transformation described by Eq. 2.62, it is defined as

$$\mathcal{L}_{kin} = \Phi^\dagger e^{qV^a t_a}\Phi. \tag{2.66}$$

The supersymmetric field-strengths are defined as

$$W_A = -\frac{1}{4}\bar{D}^2 e^{-V} D_A e^V, \tag{2.67}$$
$$\bar{W}_{\dot{A}} = -\frac{1}{4}D^2 e^{-V}\bar{D}_{\dot{A}} e^V. \tag{2.68}$$

Where the supergauge transformation of a vector-field is given by:

$$e^{V'} = e^{-i\Lambda^\dagger} e^V e^{i\Lambda} \tag{2.69}$$

It can be shown that under Eq. (2.69) the expressions $\mathrm{Tr}\,[W^A W_A]$ and $\mathrm{Tr}\,[\bar{W}_{\dot{A}} W^{\dot{A}}]$ will be invariant. If W^A is expanded in component fields, one can find the well known expression for the non-abelian field strength in the Standard-Model

$$F^a_{\mu\nu} = \partial_\mu V^a_\nu - \partial_\nu V^a_\mu + g f^a_{bc} V^b_\mu V^c_\nu. \tag{2.70}$$

Now one has what is needed in order to write down the complete SUSY-Lagrangian

$$\mathcal{L} = \Phi^\dagger e^{qV^a t_a} \Phi + W[\Phi]\bar{\theta}^2 + W[\Phi^\dagger]\theta^2 + \frac{1}{4T(R)} \mathrm{Tr}\,\left(W^A W_A\right) + \frac{1}{4T(R)} \mathrm{Tr}\,\left(\bar{W}_{\dot{A}} \bar{W}^{\dot{A}}\right). \tag{2.71}$$

Here $T(R)$ is the Dynkin index of the representation of t_a and is defined in Appendix B.

2.2.2 Soft breaking terms

There is still something missing in the total SUSY Lagrangian. If the sparticles had the same mass as their standard model particles, they would have been discovered long ago, so there must be a difference in mass between a given particle in the Standard-Model an its superpartner. In order to explain these mass differences one introduces the so-called soft terms. The name soft comes from the fact that these terms arise from a soft breaking mechanism. It has been shown that such theories are free of quadratic divergences in quantum corrections to scalar masses to all orders in perturbation theory [3].

An explicit symmetry breaking originated from an unknown spontaneous breaking mechanism is introduced in order to explain the discrepancy between SM particles and their superpartners. However, this spontaneous breaking has to happen at a much higher energy scale than the TeV scale, there exists some theories that explains how this might result in the appearance of soft terms at the TeV scale. Some of the hottest candidates for SUSY breaking models are the Planck-Scale-Mediated-Symmetry-Breaking (PSMSB) and the Gauge-Mediated-Symmetry-Breaking (GMSB). The possible soft terms are

$$\mathcal{L}_1 = -\frac{1}{4T(R)} M\theta^2\bar{\theta}^2 \mathrm{Tr}\left[W^A W_A\right] + h.c, \tag{2.72}$$

$$\mathcal{L}_2 = -\frac{1}{6} a_{ijk}\theta^2\bar{\theta}^2\Phi_i\Phi_j\Phi_k + h.c, \tag{2.73}$$

$$\mathcal{L}_3 = -\frac{1}{2} b_{ij}\theta^2\bar{\theta}^2\Phi_i\Phi_j + h.c, \tag{2.74}$$

$$\mathcal{L}_4 = -t_i\theta^2\bar{\theta}^2\Phi_i + h.c, \tag{2.75}$$

$$\mathcal{L}_5 = -m_{ij}^2\theta^2\bar{\theta}^2\Phi_i^\dagger\Phi_j, \tag{2.76}$$

$$\mathcal{L}_{soft} = L_1 + L_2 + L_3 + L_4 + L_5. \tag{2.77}$$

In addition, the term $\mathcal{L}_{maybe} = -\frac{1}{2}c_{ijk}\phi_i^\dagger\phi_j\phi_k$ that is named "maybe" because it might give rise to quadratic divergences in loop corrections if there are singlet fields in the model, and would then not be accepted as a soft term.

2.3 The MSSM

The Standard Model can be extended to involve the superpartners of the Standard Model particles and their interactions as well. There are some different extensions that can be realized, the one that has the minimal number of free fields is called the Minimal Supersymmetric Standard Model MSSM. A left handed superfield S contains a left handed Weyl spinor and a complex scalar field. To describe a Dirac fermion one needs both a left handed and a right handed Weyl spinor, so in order to explain a Dirac fermion one also introduces $\bar{T}^\dagger$ which contains a right handed Weyl spinor. The fields $S^\dagger$ and $\bar{T}$ describe the anti-fermion. Since each of the superfields contains a complex scalar field, the two superpartners of the Dirac-fermion and their antiparticles are described by these four superfields as well.

The Standard Model fermions and their corresponding superfields are shown in the Table 2.4. The right-handed neutrino fields are not included in the MSSM, they are only needed for massive neutrinos.

In addition to these fields one has the gauge fields B,W^a,C^a and the two Higgs fields H_u and H_d. As known from SM, the regular $SU(2)_L$ Higgs doublet cannot give masses to particles with isospin $I_3 = 1/2$ corresponding to the upper component of the left handed doublets, in order to achieve that one introduces the structure $H_C \equiv -i\left(H^\dagger\sigma_2\right)^T$. There is no natural way of introducing such constructions in the superpotential if one only has one Higgs doublet. One can also argue that there would appear anomalies in the tree level gauge boson couplings if only one Higgs doublet existed, but when two are introduced these anomalies cancel out. In the MSSM there are two Higgs doublets giving rise to eight d.o.f, where three of these

Superfield	L_i	$\bar{E}_i^\dagger$	Q_i	$\bar{U}_i^\dagger$	$\bar{D}_i^\dagger$
Particle	ν_{iL},l_{iL}	l_{iR}	u_{iL},d_{iL}	u_{iR}	d_{iR}
Hypercharge	-1	-2	$\frac{1}{3}$	$\frac{4}{3}$	$-\frac{2}{3}$
Superfield	$L_i^\dagger$	$\bar{E}_i$	$Q_i^\dagger$	$\bar{U}_i$	$\bar{D}_i$
Particle	$\bar{\nu}_{iR}$,l_{iR}	$\bar{l}_{iL}$	$\bar{u}_{iR}$,$\bar{d}_{iR}$	$\bar{u}_{iL}$	d_{iL}
Hypercharge	1	2	$-\frac{1}{3}$	$-\frac{4}{3}$	$\frac{2}{3}$

Table 2.4: Superfields in the MSSM with hypercharge assignment

are eaten by Z and Ws, Leading to five Higgs particles h^0,H^0,H^+,H^- and A^0. The superpartners of the Higgses are called higgsinos and the superpartners of the gauge bosons are called gauginos. These two are

$$H_u = \begin{pmatrix} H_u^+ \\ H_u^0 \end{pmatrix}, \tag{2.78}$$

$$H_d = \begin{pmatrix} H_d^0 \\ H_d^- \end{pmatrix}. \tag{2.79}$$

Two important parameters are the vacuum expectations of the charge-less parts of the Higgs fields $v_u = \langle H_u^0 \rangle$ and $v_d = \langle H_d^0 \rangle$. The parameter $\tan\beta = v_u/v_d$ is important to SUSY model structure.

To construct the MSSM Lagrangian one introduces superpotential terms, kinetic terms and gauge terms. The structure of gauge terms were obtained in section 2.2. The general kinetic terms are defined in Eq. 2.66. Now that the fields that are involved in the MSSM are known one can start to construct the Lagrangian.

$$\begin{aligned} \mathcal{L}_{kin} &= L_i^\dagger e^{\frac{1}{2}g\sigma^a W^a - \frac{1}{2}g' B} L_i + Q_i^\dagger e^{\frac{1}{2}g\sigma^a W^a + \frac{1}{2}g_s\lambda^a C^a + \frac{1}{6}g' B} Q_i \\ &\quad + U_i^\dagger e^{\frac{1}{2}g_s\lambda^a C^a - \frac{4}{6}g' B} D_i + U_i^\dagger e^{\frac{1}{2}g_s\lambda^a C^a + \frac{2}{6}g' B} D_i \\ &\quad + E_i^{\frac{2}{2}g' B} E_i + H_u^\dagger e^{\frac{1}{2}g\sigma^a W^a + \frac{1}{2}g' B} H_u + H_d^\dagger e^{\frac{1}{2}g\sigma^a W^a - \frac{1}{2}g' B} H_d. \end{aligned} \tag{2.80}$$

Here σ^a are the Pauli matrices and λ^a are the Gell-Mann matrices, which are defined in Appendix B.

The pure gauge terms can be written:

$$\mathcal{L}_V = \frac{1}{2}\mathrm{Tr}\left(W^A W_A\right)\bar{\theta}^2 + \frac{1}{2}\mathrm{Tr}\left(C^A C_A\right)\bar{\theta}^2 + \frac{1}{2}\mathrm{Tr}\left(B^A B_A\right)\bar{\theta}^2 + h.c \tag{2.81}$$

Here

$$W_A = -\frac{1}{4}\bar{D}^2 e^{-W} D_A e^W, \tag{2.82}$$

$$C_A = -\frac{1}{4}\bar{D}^2 e^{-C} D_A e^C, \tag{2.83}$$

$$B_A = -\frac{1}{4}\bar{D}^2 D_A B^0, \tag{2.84}$$

and

$$W = \frac{1}{2} g \sigma^a W^a, \tag{2.85}$$

$$C = \frac{1}{2} g_s \lambda^a C^a, \tag{2.86}$$

$$B^0 = \frac{1}{2} g^{'} B, \tag{2.87}$$

where g, $g^{'}$ and g_s are the $U(1)$,$SU(2)$ and the $SU(3)$ couplings in the SM. The terms in the superpotential must conserve hypercharge, by looking at the hypercharge of SM particles one can obtain the structure of the interactions. The abelian transformation requires that $y_i + y_j = 0$ for mass terms, $y_i + y_j + y_k = 0$ for Yukawa terms and $y = 0$ for tadpole terms. Here y is the hypercharges given by the formula $Q = I_3 + \frac{1}{2}y$, Q and I_3 are charge and isospin respectively. The superpotential takes then the following form

$$\begin{aligned} W = {} & \mu H_u H_d + \lambda^e_{ij} L_i H_d \bar{E}_j + \lambda^u_{ij} Q_i H_u \bar{U}_j + \lambda^d_{ij} Q_i H_d \bar{D}_j \\ & + \mu^{'}_i L_i H_u + \lambda_{ijk} L_i L_j \bar{E}_k + \lambda^{'}_{ijk} Li Q_j \bar{D}_k + \lambda^{''}_{ijk} \bar{U}_i \bar{D}_j \bar{D}_k. \end{aligned} \tag{2.88}$$

Where

$$H_u H_d = H_u^+ H_d^- - H_u^0 H_d^0. \tag{2.89}$$

and similar for other pairs of $SU(2)$ doublets.

The term in Eq. (2.89) is a higgsino mass term, the structure $H_u H_d$ also gives rise to the Higgs mass terms $L_{HM} = |\mu|^2 \left(|H_u^0|^2 + |H_u^+|^2 + |H_d^0|^2 + |H_d^-|^2\right)$. By comparing $H_u H_d$ and $L_i H_u$ one could speculate whether the doublet $H_d = L_i$? This leads to problems with anomaly cancellation, heavy neutrinos and lepton flavor violation at a high level. The term $L_i H_d \bar{E}_j$ gives a Yukawa interaction between a Higgs, or higgsino, to sleptons and leptons, with the constraint that both baryon and slepton number are conserved. The terms $Q_i H_u \bar{U}_j$ and $Q_i H_d \bar{d}_j$ give Yukawa couplings between a Higgs or a higgsino to squarks and quarks, with both baryon and slepton number conservation.

The last four terms in the superpotential breaks the so-called R-parity, which is defined as follows

$$R = (-1)^{2s+3B+L}\,. \tag{2.90}$$

I will return to this in section 2.5.

2.3.1 The particle content in the MSSM

Higgsinos and gauginos mix together and create two charginos and four neutralinos, while gluinos,and first and second generation squarks are assumed to not be subject of any kind of mixing. The different particles in MSSM are shown i Table 2.5, the fermion antiparticles of SM and their superpartners are not shown.

$R=1$	$R=-1$
$\gamma Z H^0 h^0\ A^0$	$\widetilde{\chi_1^0}\widetilde{\chi_2^0}\widetilde{\chi_3^0}\widetilde{\chi_4^0}$
$W^\pm H^\pm$	$\widetilde{\chi_1^\pm}\widetilde{\chi_2^\pm}$
g	$\tilde{g}$
$e^-\nu_e\mu^-\nu_\mu\nu_\tau$	$\widetilde{e_r}\widetilde{e_l}\widetilde{\nu_e}\widetilde{\nu_\mu}\widetilde{\nu_\tau}\widetilde{\mu_r}\widetilde{\mu_l}$
τ^-	$\widetilde{\tau_1}\widetilde{\tau_2}$
$udsc$	$\widetilde{u_r}\widetilde{u_l}\widetilde{d_r}\widetilde{d_l}\widetilde{s_r}\widetilde{s_l}\widetilde{c_r}\widetilde{c_l}$
b	$\widetilde{b_1}\widetilde{b_2}$
t	$\widetilde{t_1}\widetilde{t_2}$

Table 2.5: Particles and sparticles in the MSSM grouped by R-parity

The different gaugino fields that mix into free particle states are the $\tilde{B}^0$, $\tilde{W}^0$, $\tilde{W}^\pm$, $\tilde{H_u}^+$,$\tilde{H_u}^0$, $\tilde{H_d}^0$,$\tilde{H_d}^-$. Here $\tilde{B}^0$ and $\tilde{W}^0$ are the superpartners of the B^0 and the W^0, which spans out the Z-boson and the photon when rotated an angle θ_W. Generally the four neutral gaugino fields can be mixed, spanning out the Neutralinos.

$$\tilde{\chi_i}^0 = c_{i1}\tilde{B}^0 + c_{i2}\tilde{W}^0 + c_{i3}\tilde{H_u}^0 + c_{i4}\tilde{H_d}^0 \tag{2.91}$$

The two positive gaugino fields and the two negative gaugino fields can mix, spanning out two negatively and two positively charged charginos. The chargino mixing is given as

$$\tilde{\chi}^\pm = k_{1+}\tilde{W}^+ + k_{2+}\tilde{H_u}^+. \tag{2.92}$$

There is one superpartner for each left handed or right handed first and second generation fermion. In the sneutrino case only the left handed particles are contained in the MSSM. The superpartners of τ_R and τ_L can mix into $\tilde{\tau}_1$ and $\tilde{\tau}_2$. The superpartners of t_R and t_L can mix into the mass eigenstates $\tilde{t}_1$ and $\tilde{t}_2$, the same can be the case for b_R and b_L as they also have non negligible Yukawa couplings.

2.4 The SUSY breaking terms

The sfermion and gaugino mass terms in the MSSM come from the soft terms: From Eq. (2.72) one gets the gaugino terms

$$\mathcal{L}_{m1} = -\frac{1}{2}M_1\tilde{B}\tilde{B} - \frac{1}{2}M_2\tilde{W}^i\tilde{W}_i - \frac{1}{2}M_3 g^{\tilde{aA}}\tilde{g_A^a} + c.c. \tag{2.93}$$

Each of these have 2 free parameters, so they give rise to 6 free parameters in total.

From Eq. (2.73) one gets

$$\mathcal{L}_{m2} = -a^e_{ij}\tilde{L}_i H_d \tilde{e^*_{jR}} - q^u_{ij}\tilde{Q}_i H_u \tilde{u^*_{jR}} - a^d_{ij}\tilde{Q}_i H_d \tilde{d^*_{jR}} + c.c. \tag{2.94}$$

This gives rise to 54 free parameters.

From Eq. (2.74) there is one term contributing to the sfermion masses

$$\mathcal{L}_{m3} = -bH_u H_d + c.c. \tag{2.95}$$

These terms result in 2 free parameters.

From Eq. (2.76) one gets the diagonal sfermion mass terms

$$\mathcal{L}_{m4} = -m^{L2}_{ij}\tilde{L}^\dagger_i\tilde{L}_j - m^{e2}_{ij}\tilde{Q}^\dagger_i\tilde{Q}_j - m^{u2}_{ij}\tilde{u}^*_{iR}\tilde{u}_{jR} - m^{d2}_{ij}\tilde{d}^*_{iR}\tilde{d}_{jR} \tag{2.96}$$

resulting in 47 free parameters.

2.4.1 The hierarchy problem

If one tries to calculate loop corrections to the Higgs mass in the SM, one gets divergences. However, there has only been performed experiments up to a certain energy level, so one is allowed to introduce a cut of to regularize the theory, and the consequences of this are that the divergences disappear. The cut of scale would, in worst case, be at the Planck scale which is the scale where one knows that the SM does not work anymore. From the fermionic one-loop corrections shown in Fig. 2.2, and scalar one-loop corrections shown in 2.1 one gets both positive and negative contributions to the Higgs mass, with a cut of at the Planck scale the cut-off corrections are 10^{16} larger than the energy scale where measurements predict

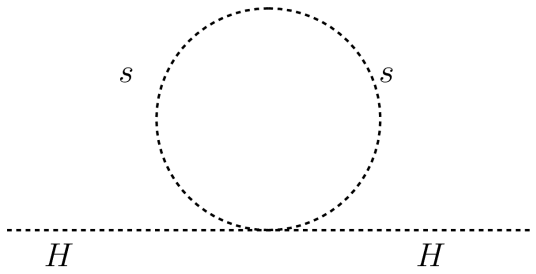

Figure 2.1: One-loop scalar contribution to Higgs mass.

the Higgs to be at. In order to have a Higgs mass of order 100 GeV, one has to introduce an enormous fine tuning.

When the experimental search for Higgs started, it was already known that it could not have a mass exceeding 1.4 TeV, because unitary would be violated for certain scattering processes. As the experimental search proceeded the limits were narrowed down, the LEP experiments [8] sat a lower bound for the Higgs mass at 114.1 GeV at confidence level of 95 %. Nowadays the diphoton search at ATLAS experiment [9] has placed the Higgs mass in the range 115–134.5 GeV at a 95% confidence level, while CMS collaboration [10] has excluded a SM Higgs boson in the range 127–600 GeV at a 95% confidence level. The total one-loop corrections to the Higgs mass is

$$\Delta m_h^2 = -\frac{|\lambda_f|^2}{8\pi^2}\Lambda_{uv}^2 + \frac{\lambda_s}{16\pi^2}\Lambda_{uv}^2, \tag{2.97}$$

where Λ_{uv} is the cut-off scale. The particles that dominates this contribution to the Higgs mass in SUSY are the top-quark and the stop-squark, this is because they have a much larger Yukawa coupling than other quarks and squarks. In unbroken SUSY one has that

$$|\lambda_f|^2 = \lambda_s. \tag{2.98}$$

SUSY also predicts that there should be twice as many scalars as fermions, so unbroken SUSY predicts an exact cancellation and does not introduce any fine tuning at all. However, as mentioned earlier SUSY must be broken and the cancellation is

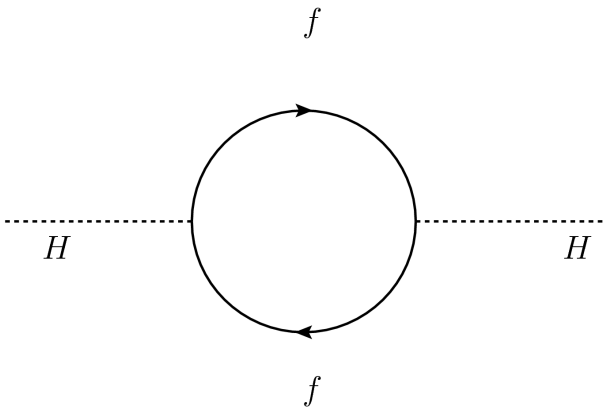

Figure 2.2: One-loop fermion contribution to Higgs mass.

not exact, from this the little hierarchy problem arises. The soft terms contribute at most

$$\Delta m_h^2 = -\frac{\lambda_s}{16\pi^2} m_s^2 \ln \frac{\Lambda_{uv}^2}{m_s^2}. \tag{2.99}$$

Here m_s are the masses of the scalar SUSY particles. According to the formula above, m_s cannot be too large compared to the Higgs mass, in order to avoid getting corrections that blow up, which is one of the reasons for believing that SUSY is manifested at the TeV scale.

2.4.2 The gluino

The Gluino is a fermion, it is believed to be a majorana fermion, which means that it is its own anti-particle. Because it is the superpartner of the gluon it inherits the color octet structure. It has nothing to mix with so its mass is mainly defined by the strong mass parameter M_3. It also gets some of its mass from loop corrections discussed in the SUSY primer [3]. The loop corrections that are shown in Figure 2.3 and 2.4 give rise to the corrections

$$m_{\tilde{g}} = M_3(\mu)\left[1 + \frac{\alpha_s}{4\pi}\left(15 + 6\ln\left(\frac{\mu}{M_3}\right) + \Sigma A_q\right)\right], \tag{2.100}$$

where

$$\Sigma A_q = \int_0^1 x ln\left(\frac{x m_{\tilde{q}}^2}{M_3^2} + 1 - x\frac{m_q^2}{M_3^2} - x(1-x) - i\epsilon\right) \mathrm{d}x. \tag{2.101}$$

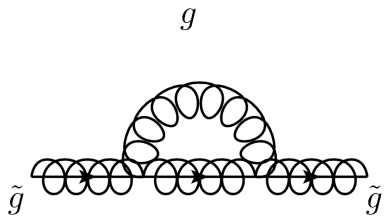

Figure 2.3: One-loop correction to the gluino mass

Here α_s is the strong coupling, $m_{\tilde{q}}$ are squark masses and m_q are the corresponding quark masses, while μ is the energy scale of the renormalization. The sum is taken over all 12 squark-quark supermultiplets. The numerical factor 15 comes from the color nature of the gluino. In gauge coupling unification models the following relations are satisfied

$$M_3 = \frac{\alpha_s}{\alpha} \sin^2 \theta_W M_2 \tag{2.102}$$

$$M_3 = \frac{3}{5} \frac{\alpha_s}{\alpha} \cos^2 \theta_W M_1. \tag{2.103}$$

This approximately gives: $M_3 : M_2 : M_1 = 6 : 2 : 1$, so in this scheme it is reasonable to believe that the gluino is heavier than the charginos and the neutralinos. In my study described in chapter 3, either the squarks or the gluinos are assumed to be the Next-to-Lightest-Supersymmetric-Particle (NLSP), which means that in this model there is no gauge coupling unification.

2.4.3 The squarks

The squarks are spin–0 particles and carry baryon number, flavor, color and charge. The diagonal mass terms are

$$\mathcal{L}_{1L} = -m_F^2 F_i^\dagger F_i, \tag{2.104}$$

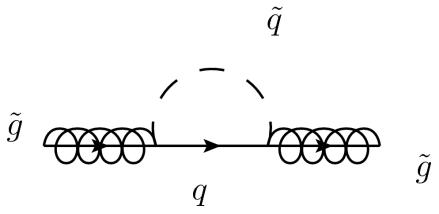

Figure 2.4: One-loop correction to the gluino mass

$$\mathcal{L}_{1R} = -m_f^2 \tilde{f}_{iR}^* \tilde{f}_{iR}, \tag{2.105}$$

for the squarks in the left handed doublets and the right handed singlets respectively. The hyperfine terms that come from the ElectroWeak Symmetry Breaking (EWSB) and the D-term breaking gives rise to the following mass terms, D-terms are removed by use of Euler-Lagrange's equation, giving rise to terms in the scalar potential, it can be showed that SUSY is broken when the minimum of this scalar potential is greater than zero [3].

$$\Delta_f = \left(I_{3F} g^2 - Y_F g'^2 \right) \left(v_d^2 - v_u^2 \right) \tag{2.106}$$

There are also some F-term contributions after EWSB that comes from Yukawa terms in the superpotential that give rise to mass terms on the form

$$\mathcal{L}_{2L} = \left(v_{u/d} y_f \right)^2 \tilde{f}_{iL}^* \tilde{f}_{iL}. \tag{2.107}$$

and

$$\mathcal{L}_{2R} = \left(v_{u/d} y_f \right)^2 \tilde{f}_{iR}^* \tilde{f}_{iR}. \tag{2.108}$$

These are only important for large Yukawa couplings y_f, so they can be neglected for first and second generation squarks due to the inheritance of Yukawa couplings. In addition there are also some F-terms that combine scalars from the $\mu H_u H_d$ and Yukawa terms with a Higgs Vacuum expectation value (VEV), which give mas terms

$$\mathcal{L}_{3RL} = -\mu^* v_{u/d} y_f \tilde{f}_R^* \tilde{f}_L + c.c. \tag{2.109}$$

Finally, there are some mass terms

$$\mathcal{L}_{4RL} = a_f v_{u/d} \tilde{f}_L \tilde{f}_R^* + c.c \tag{2.110}$$

coming from soft breaking Yukawa terms with F fields and a Higgs VEV. Where one often assumes that $a_f = A_f y_f$. For first and second generation squarks the main contributions come from Eq. (2.04), Eq. (2.05), and Eq. (2.06).

2.4.4 Bounds on masses in the R-parity conserving case

The ATLAS collaboration [11] at CERN has excluded important mass scenarios in the R-parity conserving case. Here μ is the coupling linked to the higgsino mass term in the superpotential, while A_0 is a parameter related to the scale of the symmetry breaking. The study assumes that $\tan\beta = 10$, $A_0 = 0$, $\mu > 0$ for 1.04fb^{-1} data. When $m_{\tilde{g}} = m_{\tilde{q}}$ in the mSUGRA model the conclusion is that

$$m_{\tilde{q}} > 950 \text{ GeV} \tag{2.111}$$

$$m_{\tilde{g}} > 950 \text{ GeV}. \tag{2.112}$$

When the search assumes that $m_{\tilde{g}} \neq m_{\tilde{q}}$ they got the following constraints

$$m_{\tilde{q}} > 875 \text{ GeV} \tag{2.113}$$

$$m_{\tilde{g}} > 700 \text{ GeV}. \tag{2.114}$$

As mentioned earlier the focus of this thesis has been to set boundaries on squark and gluino masses in the RPV scheme. These results are presented in Chapter 3 and the limits turns out to be much weaker than what is achieved by the ATLAS collaboration for the R-parity conserving (RPC) case.

2.4.5 Dark matter

Dark matter is a type of matter that does not interact electromagnetically. The analysis of galactic motion done by Zwicky in 1933 [12] suggested the existence of non-luminous matter in addition to the known matter, confirmed much later by a

study done by Vera Rubin [13] on rotational curves for galaxies. Nowadays there are many studies in cosmology that support their conclusions. The dark matter is believed to be the dominant type of matter in the universe. One distinguishes between cold and hot dark matter. Earlier either one was not preferred but now the cold dark matter theories are favoured due to cosmological measurements. The three most important cold dark matter candidates are the Massive Compact Halo Objects (MACHOS), axions, and the Weakly Interacting Massive Particles (WIMPs). The MACHOS are large condensed objects believed to be the size of planets. The most important strategy in the search for MACHOS is to look at effects from gravitational lensing. Axions are very light particles that are introduced in order to explain why QCD does not break CP-symmetry. WIMPs are massive particles that interact trough the weak force and gravitation. Since WIMPs do not interact with either the strong nuclear force or electromagnetism, they behave like massive neutrinos.

The dark matter candidate in RPV scenarios has to be extremely weakly interacting, otherwise it would rapidly decay. The candidates that are favoured to constitute dark matter are the gravitiono and the axino. The axino is the superpartner of the axion. The gravitino is the superpartner of the graviton and it obeys spin–3/2 statistics. However, there has never been discovered any spin–3/2 particle, so where is it? As implied earlier the gravitino is a weakly interacting particle with scattering amplitudes at 10^{-19} GeV^{-1} and hence negligible in collider experiments. The gravitinos are assumed to have been created from the (NLSP) decay or in thermal production $gg \to g \to \tilde{g}\tilde{G}$ at reheating after the cosmic inflation. The gravitino decay is suppressed by the Planck mass and hence gravitinos are long lived even in RPV models.

It is even conceivable that colored particles like squarks and gluons could form bound colorless particles, which again would constitute dark matter, given that they exist, they have to be hadrons, leading to the name R-hadrons. R-hadrons would consist of at least one squark with other colored particles, or at least one gluino with other colored particles. R-hadrons are possible when a colored supersymmetric particle has a mean lifetime that is longer than the hadronization time. The hadronization time is the time it takes for a colored particle to form a bound state together with colored particles of the vacuum. R-hadrons can be systematized into R-mesons, R-baryons and gluinoballs. R-mesons consist either of $\widetilde{g}\bar{q}q$ or $\widetilde{q}\bar{q}$, R-baryons consist either of $\widetilde{g}qqq$ or $\widetilde{q}qq$, and gluinoballs consist of $\widetilde{g}g$. In the R-parity violating theories the squarks and gluinos typically have a lifetime that is shorter than the hadronization time, so then it is not possible to have R-hadrons.However, if R-parity is very weakly broken, then the colored sparticles could have lifetimes that are longer than the hadronization time, and formation of R-hadrons might be

possible.

2.5 R-Parity violating SUSY

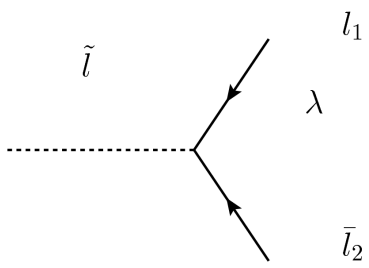

Figure 2.5: Generic vertex for the LLE coupling, which breaks lepton number.

The appearance of R-parity violating couplings has been discussed for some decades. The major problem is that this break lepton or/and baryon number. They must be considered even in the R-parity conserving theories, because they arise in the superpotential in a natural way. Hence these theories must justify why the R-parity violating terms are omitted.

From searches at the LHC it seems that the sparticles in the RPC scheme have to be close to 1 TeV, this is not the case in the RPV scenario at the present, which motivates the study of this scenario, but there are some problems that must be coped with, including the stability of the proton. These theories might also solve some problems, for instance they provide a LSP candidate, which is weakly interacting, and hence a good candidate to constitute cold dark matter, although it would not be stable.

The RPV terms in the superpotential are the four last terms in Eq. (2.88). They give rise to interactions shown in Fig. 2.5, Fig. 2.6 and Fig. 2.7

These couplings break baryon and/or lepton number conservation, they allow the superpartners to decay into final states that contain only SM particles, they also affect parameters that are studied in precision experiments. From this, one can set

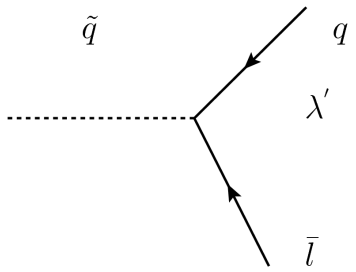

Figure 2.6: Generic vertex for the LQD coupling,which breaks lepton number

limits on the R-parity violating couplings. By requiring gauge invariance one gets the following

$$\lambda_{ijk} = -\lambda_{jik}, \tag{2.115}$$

and

$$\lambda''_{ijk} = -\lambda''_{ikj}. \tag{2.116}$$

The LLE, LQD and LH couplings violate lepton number (L) conservation, while the UDD coupling violate baryon number conservation. There are 3 potential bilinear μ'_i couplings which mixes charged leptons with down type Higgses and breaks lepton number. In the trilinear domain there are 9 λ_{ijk}, 27 λ'_{ijk} couplings that break lepton number conservation and 9 λ''_{ijk} that break baryon number conservation. In addition to the superpotential terms, there are also the soft breaking R-parity violating terms. These terms introduce about 100 free parameters, some of these parameters can be eliminated, which parameters can be eliminated depends on the basis chosen.

2.5.1 Proton decay

One can set boundaries on some of the trilinear couplings by looking at the proton decay to $e^+\pi^0$. By making use of the couplings λ'_{ijk} and λ''_{ijk}, d and u quarks in the proton could fuse together into a scalar particle, that once more could split into a lepton and a quark shown in Fig 2.8. From experiments one knows that the

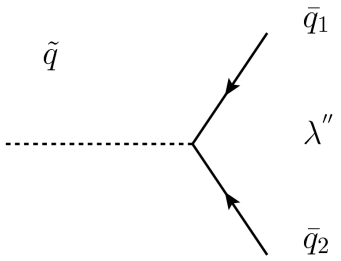

Figure 2.7: Generic vertex for the UDD coupling, which breaks baryon number.

lifetime of the proton must be greater than 6.6×10^{33} years [14], which corresponds to decay rate less than 1.35×10^{-35} GeV. By analyzing the Feynman diagram involved and assuming that the mass of the intermediate particle is 1 TeV, one gets that $\lambda'_{ijk}\lambda''_{11l} < O\left(10^{-12}\right)$, here λ'_{ijk} and λ''_{11l} are the involved couplings. The limit is set on the product of two different couplings, so this does not imply that it is a limit on the dominant coupling.

2.5.2 Experimental search for R-parity violation at hadron colliders

The way SUSY can be discovered at colliders crucially depends on the structure of the model followed by nature. RPV and RPC models could have different signals at colliders, hence the search strategy in these two scenarios must be different as well. The phenomenology at colliders in the RPV case turns out to be highly dependent of couplings, so that for a wide range of couplings the manifestation of RPV SUSY would be indistinguishable from the RPC case.

Most of the SUSY searches that has been performed the last years have been done in the RPC scheme, but the RPV scenario gets more and more interesting to study, as larger and larger parts of the parameter space in the RPC theories are ruled out. The majority of limitations on the parameters of the sparticles come from the experimental search at Tevatron, Hera and LEP summarized in the PDG [15]. In most SUSY models a stable LSP is believed to constitute the dark matter, so naturally a lot of experiments that have been performed have focused on the LSP. The production of LSP will lead to missing momentum signals which differ

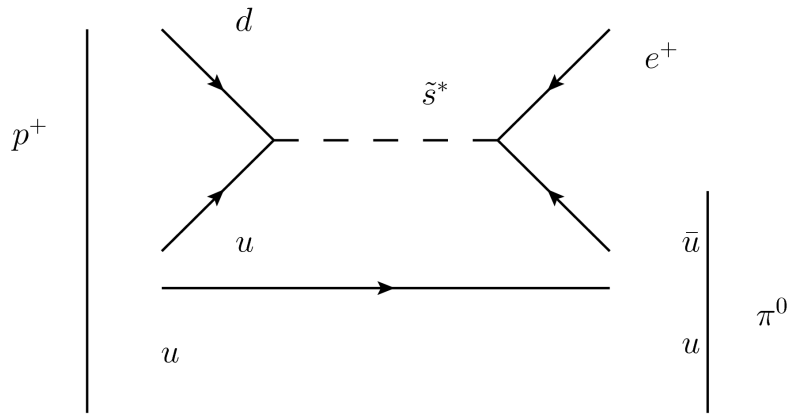

Figure 2.8: Diagram contributing to proton decay through the couplings $\lambda^{'}_{112}$ and $\lambda^{''}_{112}$.

from the signals in the RPC case. In the RPC scenario, the produced particles must decay in cascades resulting in final states that contain the LSP and SM particles. In addition, supersymmetric particles (sparticles) must be produced in pairs. While the presence of R-parity violation affects the phenomenology in supersymmetry searches, by opening up for decay and production channels that are not allowed in the RPC case, e.g allowing single production of SUSY-particles.

In the RPV theories some of the trilinear couplings can be different from zero and hence the supersymmetric particles are allowed to decay directly into final states containing only standard model particles. For sparticles other than the LSP these direct decays might be just as important as the cascade decays when it comes to excluding areas in parameter space. In most of the RPV models with dark matter the gravitino is assumed to be the LSP. Due to the fact that the gravitino interaction is suppressed by the Planck mass M_p it cannot be discovered directly at colliders, which makes the search for the NLSP important.

There are 45 independent trilinear couplings λ_{ijk}, $\lambda^{'}_{ijk}$ and $\lambda^{''}_{ijk}$, and dealing with the task of testing all the combinations of these possible non-vanishing coupling combinations, one assumes a strong hierarchy among the couplings. One postulates that one of the couplings is more dominant than the others in order to simplify the experimental search, this coupling is named Λ. In order to optimize the search, strategies must take into account bounds on Λ from precision measurements.

If Λ were to be less than 10^{-6}, the NLSP would be stable in an experiment. For values of $\Lambda > 10^{-2}$ the decay rate would be so large that there would be single particle production. A possible search strategy in such cases, in this regime, is to

neglect R-parity contributions at production channels, this can be done if the RPV couplings are small compared to RPC couplings.

As in the RPC scenario the study of gluinos and squarks at hadron colliders are very interesting when it comes to setting boundaries on the parameter space. This is because gluinos and squarks are colored objects and hence their production cross-section will be dominant compared to other SUSY particles.

In the study I have performed, which is described in Chapter 3 and 4 I have looked at different squark and gluino masses on a grid where the lightest of them were assumed to be the NLSP. The dominant coupling can take values in the range $10^{-6} < \Lambda < 10^{-2}$, so the production is dominated by interactions that conserves R-Parity. If the gravitino is the LSP, then the decay from the NLSP to a final state containing the LSP through a RPC coupling is suppressed by M_p. So then the NLSP will mainly decay through RPV couplings.

Chapter 3

Production of squarks and gluinos at the LHC

The main focus of this study is to constrain squark and gluino masses given that there is a dominant baryon number violating RPV coupling $\lambda^{''}$ in the range $10^{-6} < \lambda^{''} < 10^{-2}$ and that squarks and gluinos are the lightest sparticles except for the gravitino. Squarks and gluinos are assumed to be produced in proton-proton collisions and can further on decay through R-parity violating channels. The decay products become hadronic jets. These will be investigated in Monte Carlo simulations by looking for peaks at the points where the squark and gluino mass are determined to be. A fit to these peaks will be performed, which will be used in the further $\Delta\chi^2$ analysis that finally will be used to exclude certain squark and gluino mass scenarios. A data set for QCD backgrounds and a corresponding fit to the data which are important components of the $\Delta\chi^2$ analysis have been adopted from the article [1].

3.1 A Search done by the CMS collaboration

The main focus of my thesis has been to expand the search for 3-jet resonances from gluino decay done in [1] to involve squark decay as well. This study assumes production of gluinos from proton-proton collisions at 7 TeV, where the gluinos are constrained to decay into 3 quarks. This study used a 35.1 pb^{-1} of data.

From QCD one knows that colored particles cannot exist freely in nature, but they can be combined with other colored objects, forming a bound state with zero color. Colored objects produced in decays at colliders will combine with other colored objects that are produced in the same collision. The objects are called hadronic jets and can be seen as energy deposits in the detectors. In numerical simulations jets can be found by the use of a jet-algorithm.

In this analysis the anti-k_T algorithm [16] has been used to reconstruct the jets, here the cone radius is set to 0.5. Events with 6 or more jets are kept and the 6 jets with the highest transverse momentum are arranged into triplets. Each of these jets is required to have transverse momentum greater than 45 GeV and absolute pseudorapidity less than 3. In addition the transverse momentum of all the jets in the final state combined is required to exceed 425 GeV. The transverse momentum used here is the component of the momentum perpendicular to the beam axis. When θ is the angle between a massless particle direction and the beam axis the pseudorapidity is given as $\eta = -\ln(\theta/2)$. Then, assuming that each of the produced gluinos resulted in quarks contained in one of these 20 triplets, this makes the remaining 18 triplets as background. This combinatorial background is not to be confused with regular QCD background.

In order to pick out the signal triplets one requires that the invariant mass of the triplets has to be less than the sum of the absolute value in transverse momentum for each jet minus a variable Δ.

$$M_{jjj} < \sum_{i=1}^{3} \mid p_T^{jet} \mid -\Delta. \tag{3.1}$$

Here Δ is a parameter that can be adjusted to optimize the selection. In the CMS analysis Δ is set to 130 GeV. After this selection is performed, a considerable amount of background from both the uncorrelated triplets in signal events and the regular QCD processes remains.

The QCD background is the dominant one. A rescaled mass distribution of triplets form events with $N_{jet} = 4$ and is used to estimate the shape of the background. The M_{jjj} distribution of these triplets is multiplied by the ratio of the average triplet scalar p_T in data, for the $N_{jet} > 5$ to the $N_{jet} = 4$ region to account for expected minor kinematical differences between the two regions. The resulting M_{jjj} distribution is then parametrized with the following exponential function

$$f(x) = e^{A+Bx}, \tag{3.2}$$

where $A = 5.6$ and $B = -0.0067$. Simulated events that satisfy the selection criteria above are plotted against their 3-jet invariant mass for a model with $m_{\tilde{g}} = 250$ GeV, together with data points and the exponential fit function in Fig. 3.6. A maximum likelihood analysis is performed for the signal, the exponential fit function and the data points, resulting in an exclusion plot of the cross section at 95 % confidence level with the actual cross sections shown in Fig. 3.1. The model is excluded at 95% C.L for a given gluino mass when the observed cross section limit at 95 % C.L lies below the MSSM cross section, excluding gluino masses in the range 200–280 GeV.

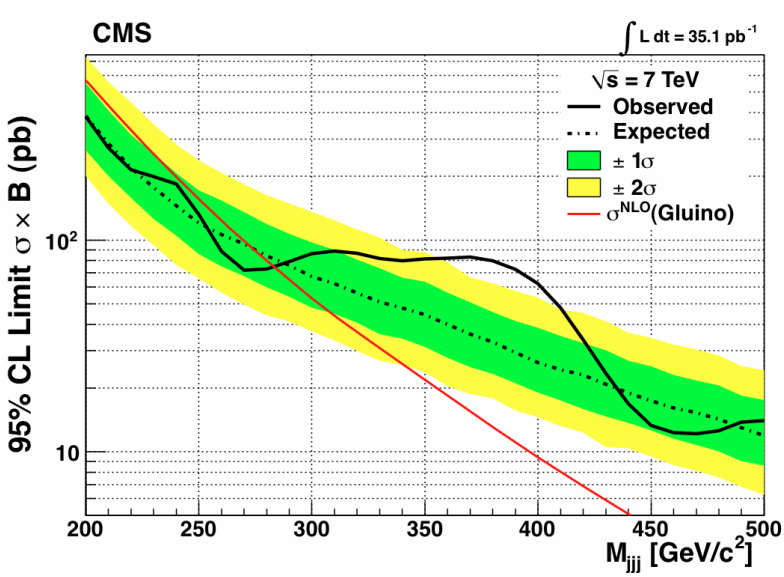

Figure 3.1: Cross section limits at 95% C.L set by the CMS collaboration [1]

3.1.1 The anti-kt jet algorithm

A jet is a shower of hadrons originated from a shower of quarks and gluons through hadronization. At hadron-colliders quarks and gluons cannot be detected directly, the quantities that can be detected are the jets. These are registered in the hadronic calorimeter. Jet algorithms are used both in event reconstruction at hadron colliders and in simulations of hadron collisions. The purpose of the jet algorithm is to identify jets and find the kinematical properties of them, such as energy, momentum and pseudorapidity as close as possible to the same properties for the quark and gluon that the originates from.

The anti-KT algorithm is a clustering algorithm, clustering algorithms reconstruct jets by pair-wise grouping together nearby objects. The anti-KT algorithm combine highest p_T objects first. The algorithm starts with a list of final state objects. For each object i one defines

$$d_i \equiv p_{Ti}^{-2}. \tag{3.3}$$

For each pair of objects one defines

$$d_{ij} \equiv \min\left(p_{Ti}^{-2}, p_{Tj}^{-2}\right) \frac{\Delta_{ij}^2}{R^2} \tag{3.4}$$

where R is the cone radius and

$$\Delta_{ij}^2 = (y_i - y_j)^2 + (\phi_i - \phi_j)^2, \tag{3.5}$$

y and ϕ are the rapidity and the azimuth respectively. Then the algorithm finds the minimum of all d_i and d_{ij}. If d_{ij} is the minimum then objects i and j are merged into a new object. If d_i is the minimum then object i is considered a jet. This procedure is repeated until no objects remain.

3.2 In search of 3-jet resonances from squark and gluino decay

Now the analysis performed in [1] is extended to involve production and decay of squarks. I have looked at production of squarks and gluinos in proton–proton collisions at 7 TeV. I have used Herwig++ 2.5.1 [17] to simulate this production. This program is a Monte Carlo event generator which simulates both lepton–lepton and hadron–hadron collisions. Herwig++ also handles the decay of squarks and gluinos and takes care of the hadronization of the decay products. The program also takes into account both final and initial state radiation. The squarks involved in this study are $\tilde{u}_R$,$\tilde{u}_R^*$, $\tilde{d}_R$ and $\tilde{d}_R^*$ giving a conservative bound on squark production. When $m_{\tilde{q}} < m_{\tilde{g}}$ the gluino must decay into 3 quarks through RPV coupling, and when $m_{\tilde{q}} < m_{\tilde{g}}$ it mainly will decay into a gluon and a squark. When $m_{\tilde{q}} > m_{\tilde{g}}$ the squark must decay into two quarks, and when $m_{\tilde{q}} > m_{\tilde{g}}$ the squark mainly decays into a quark and a gluino.

The squarks and gluinos are assumed to be so heavy that they can decay into states of multiple quarks. In this study I vary in having gluinos or squarks as the NLSP. What is important, as discussed in the decay chapter, is that the when the gravitino or the axino are assumed to be the LSP, then the decay into these are suppressed so the R-parity violating decay are the dominant one. So that is the only one affecting the lifetime of the NLSP. Also because the NLSP must decay through the R-parity violating coupling the observables are insensitive to the value of $\lambda^{''}$ in the range $10^{-6} < \lambda^{''} < 10^{-2}$. The final states will mainly contain quarks and gluons, and these will become jets trough hadronization processes. I have used FastJet [18] and the anti-KT algorithm [16] to find jets that are produced in Herwig++. Decay tables and masses are obtained by reading in Susy Les Houches Accord (SLHA) files [19]. The selection criteria for jets, QCD background and an integrated luminosity of 35.1 pb^{-1}, are inherited from the article [1] by the CMS collaboration.

There is a small splitting between $m_{\tilde{u}_R}$ and $m_{\tilde{d}_R}$ in the SLHA files created from the mass grid. The hyperfine splitting term in Eq. (2.106) gives rise to this splitting due to the difference in charge between the particles. The mass grid values are given by the soft mass (SUSY breaking) parameters $m_{\tilde{u}_3} = m_{\tilde{d}_3} = m_3$, which is the parameter I set bounds on, while both particles get the same one-loop correction to their mass. For $m_3 = 200$ GeV the hyperfine splitting is about 5 GeV and the

one-loop correction is of order 10 GeV giving the physical masses $m_{\tilde{u}_R} \approx 205$ GeV and $m_{\tilde{d}_R} \approx 210$ GeV.

The coupling $\lambda^{''}$ is assumed to be in the range 10^{-2}–10^{-6}. The lower limits comes from the fact that the particle has to decay before it reaches the detector, otherwise it would not be possible to register hadronic jets in the detector. it is reasonable to assume that

$$\Gamma \approx |\lambda^{''}|^2 m \tag{3.6}$$

where m is the mass of the decaying particle. The lifetime of the particle is given as

$$\tau = \frac{\hbar}{\Gamma}. \tag{3.7}$$

Thus

$$|\lambda^{''}| \approx \sqrt{\frac{\hbar}{\tau m}}. \tag{3.8}$$

The distance from the point of collision to the detector is approximately 5 cm and the speed of the decaying particle is of order speed of light, which implies $\tau \approx 10^{-10}$. Then if the mass is of order 100 GeV, one gets that:

$$|\lambda^{''}| \approx \sqrt{\frac{10^{-16}}{10^{-10}10^{11}}} \approx 10^{-7.5} \tag{3.9}$$

The review article [4] operate with a lower value of $\lambda^{''}$ of 10^{-6}. This is a reasonable agreement since a non-prompt decay can be identified from tracks originating some distance before the detector.

If one look at the production of squarks and gluinos at LHC the most important production channels are the following

- $gg \rightarrow \tilde{g}\tilde{g}$,$\tilde{q}_i\tilde{q}_j{}^*$
- $qg \rightarrow \tilde{g}\tilde{q}_i$
- $q\bar{q} \rightarrow \tilde{g}\tilde{g}$,$\tilde{q}_i\tilde{q}_j{}^*$
- $qq \rightarrow \tilde{q}_j\tilde{q}_i$

The leading order Feynman diagrams describing these processes are shown in Fig. 3.2 and Fig. 3.3.

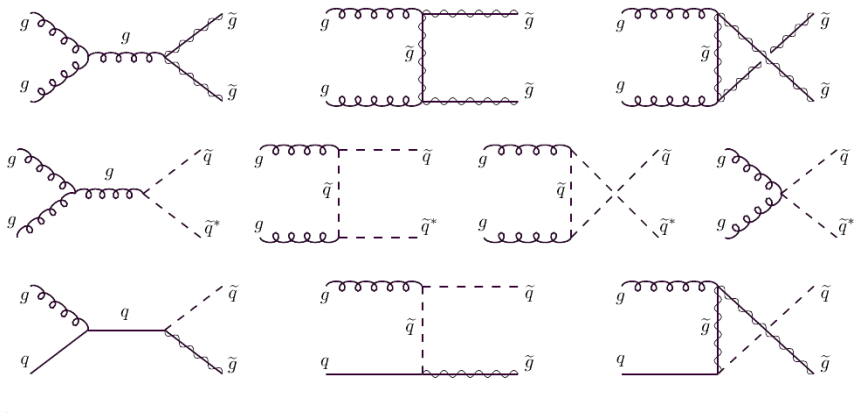

Figure 3.2: Feynman diagrams for squark and gluino production through gluon-gluon fusion and gluon-quark fusion taken from A Supersymmetry Primer [3]

3.2.1 Event generation

I have looked at gluino and squark masses on a grid in the range 160 GeV to 420 GeV. The reason for choosing 160 GeV as lower limits is because the article [1] excluded a model with gluinos in the range 200–280 GeV. The upper limit in masses is chosen to be 420 GeV, this is because it is clear that the model cannot be excluded any longer when gluino and squark masses reach this value as we will see in figure 3.8. The grid resolution is 20 GeV, so the total number of mass scenarios are 196. This search according to [1] assumes that gluinos and squarks are produced giving rise to at least 6 final state jets. The produced neutrinos are omitted from the event because they cannot be detected at LHC and are therefore considered missing energy.

For each grid point, I have chosen to generate 500000 events with the Monte-Carlo generator, where a few thousand events survives the selection criteria introduced by [1]. As mentioned the number of events is plotted against the 3-jet invariant mass, this plot contains peaks around both the gluino mass and the squark mass. A plot for masses $m_{\tilde{g}} = 400$ GeV and $m_{\tilde{q}} = 260$ GeV, with belonging fits shown in Fig 3.4. The fits are performed in the regions 255.5–284.5 GeV for $m_{\tilde{q}}$ and 384.5–407.5 GeV for $m_{\tilde{g}}$. The selection criteria eliminates a lot of the combinatorial background, so the peaks are not smeared out, and hence easy to distinguish from each other as long as the gluino mass is not close to the squark mass. A Gaussian fit is done to the peaks in order to determine the expected shape and normalization, and this fit is used in the further statistical analysis. The fit procedure is most difficult when the squark and gluino mass differ by 20 GeV, this is because the excitations overlap. In the further statistical analysis the fits to both the gluino

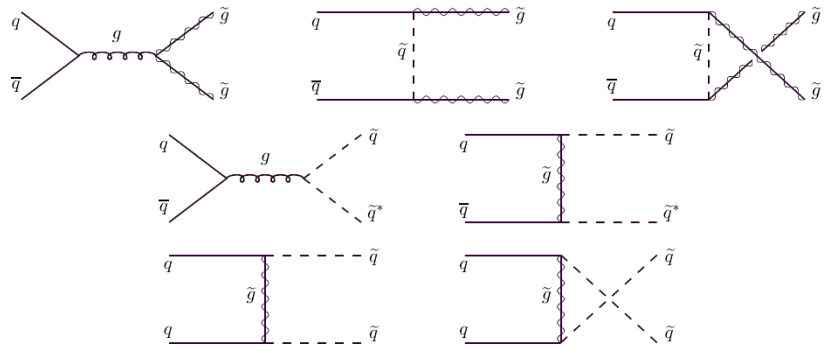

Figure 3.3: Feynman diagrams for squark and gluino production through quark-quark fusion taken from— A Supersymmetry Primer [3]

excitation and the squark excitation are normalized to the Next-to-Leading-Order (NLO) order cross section generated by Prospino [20]. Prospino is a Fortran program that calculates both Leading Order and NLO production cross section for squarks and gluinos at hadron colliders. The ratio between NLO and LO cross sections for the 196 grid points were located in the range 1.4–1.8.

I have also reproduced the results obtained by the CMS collaboration in their study [1]. This is done to ensure that the procedure that is used in my analysis is not biased. In this analysis only the gluinos were produced as in the study by the CMS collaboration [1]. The gluino pairs produced by Herwig++ were constrained to decay into 3 quarks trough R-parity violating couplings. In Herwig++[17] this is incorporated by reading in SLHA files [19], which contain SUSY and Standard Model parameters, masses and decays tables. The jet triplets that survive the selection criteria described in [1] are as an example plotted against M_{jjj}.

A plot of the three jet invariant mass distribution for a gluino with mass 280 GeV is shown in Fig 3.5. The plot is created from an analysis with 250000 events in Herwig++. From the plot one can see that the peak is located around $M_{jjj} = 280$ GeV as expected. The plot also contain a fit which is of importance in the further delta-chi-square analysis. This Gaussian fit has been performed in the region 268.1–287.9 GeV. I have used 6/GeV bins in the plots where the fit has been performed. Later on, the fit is rescaled in order to be comparable with the background that is binned with 10/GeV. In this analysis I scale my signal with a factor n, which is the free parameter in this analysis. The theoretical model consists of both the scaled signal and the exponential fit-function.

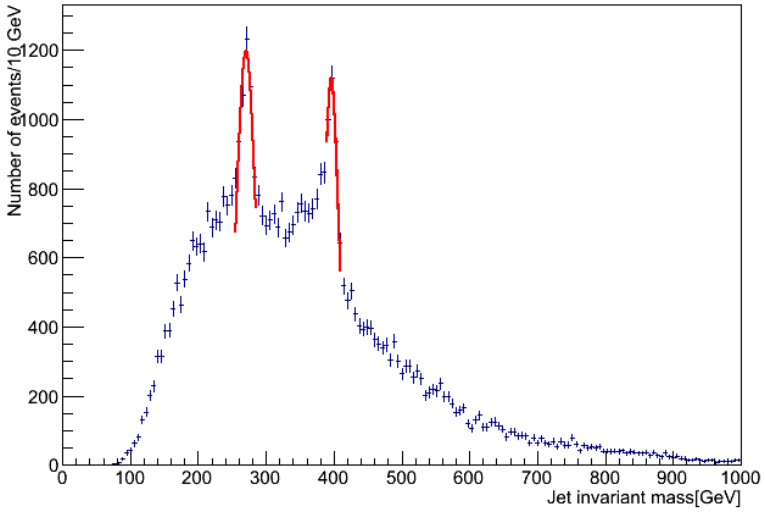

Figure 3.4: Number of signal triplets for model with peaks at $m_{\tilde{g}} = 400$ GeV and $m_{\tilde{q}} = 260$ GeV as a function of invariant mass. Two Gaussian fits to the resonances are also shown in the plot.

3.3 The statistical procedure

Now the $\Delta\chi^2$ analysis is used to obtain constraints on squark and gluino masses in the assumed model. The expression for the χ^2 is the following.

$$\chi^2 = \sum_{i=1}^{59} \frac{(O_i - F_T)^2}{\delta_i^2}, \tag{3.10}$$

where the theoretical model is given by

$$F_T(x) = f(x) + n f_s^{\tilde{g}}(x) + n f_s^{\tilde{q}}(x). \tag{3.11}$$

The function f and the CMS data points O_i are shown in Fig. 3.6 taken from the article[1]. Here, F_T is the total signal that is compared to the data points in the $\Delta\chi^2$ analysis. The quantities $f_s^{\tilde{g}}$ and $f_s^{\tilde{g}}$ are the gluino peak and the squark peak contributions respectively. The function f is described in Eq. (3.2). The quantities δ_i are the error on the data points. The parameter n is a free parameter that scales the signal.

I now want to find the value of n when $\Delta\chi^2$ has exceeded a value $\Delta\chi^2 = 3.84$ at the right side of the minima for χ^2, this corresponds to a p-value of 5%. These are the ingredient in a so-called one tailed chi squared test, the p-value is the probability

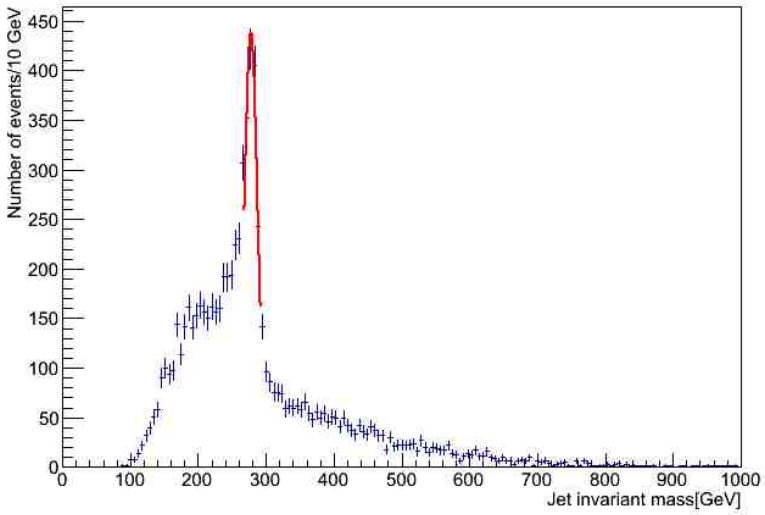

Figure 3.5: Three jet invariant mass distribution for a gluino with mass 280 GeV with a Gaussian fit.

of having a test statistic at least as extreme as the one observed. The χ^2 is calculated for F_T with the CMS data points. This is done for 59 data points in the range 165 GeV to 805 GeV with a resolution of 10 GeV. As an example the χ^2 as a function of n is shown for $m_{\tilde{g}} = 260$ GeV and $m_{\tilde{q}} = 220$ in Fig. 3.7. This minimization procedure was performed using the MIGRAD algorithm in the package TMinuit [21].

The scaling factor n is found for every mass point in the grid and is plotted in a Fig. 3.8 against both squark and gluino mass. The model is then excluded at 95% C.L where this scaling factor is below 1, as the signal would be too large compared to the background.

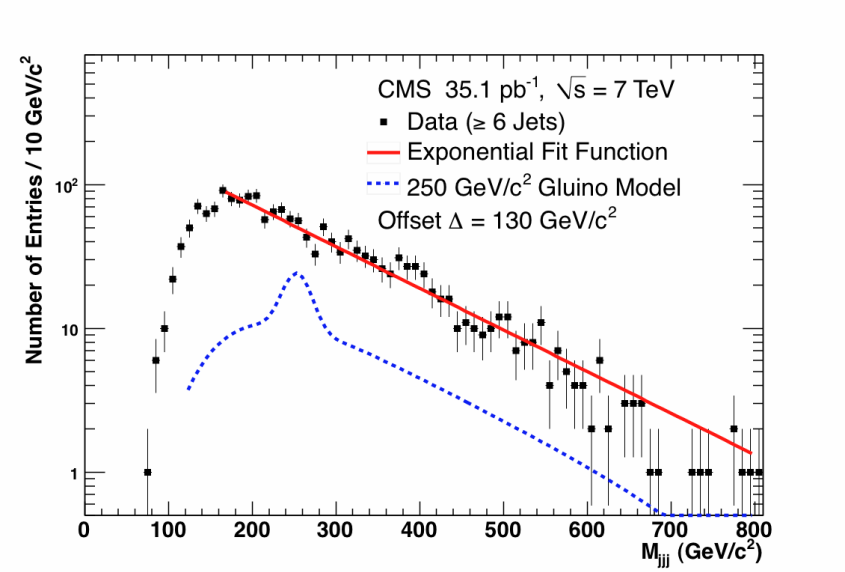

Figure 3.6: Plot of CMS data and the background model found in [1]

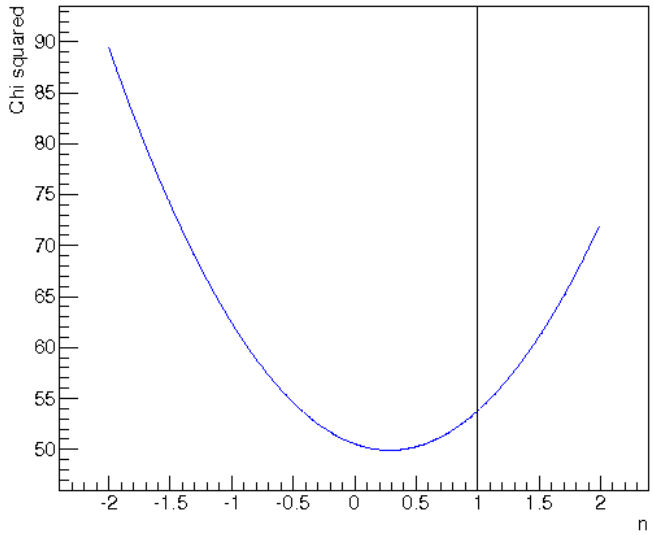

Figure 3.7: Chi square is plotted against n for $m_{\tilde{g}} = 260$ Gev And $m_{\tilde{q}} = 220$ GeV, the line where exclusion of the model starts is located at $n = 0.9986$.

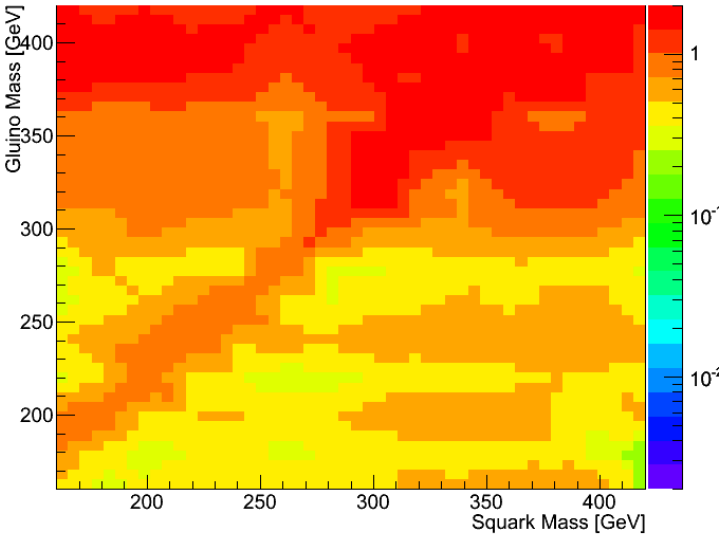

Figure 3.8: Scaling factor n at 95% C.L.

The areas in Fig. 3.8 that are not excluded are light red or red. All values above 2 are set to be red, while those below 0.002 are set to be light green. The number of points in both $m_{\tilde{q}}$ and $m_{\tilde{g}}$ direction are set to 50. Originally there were 14 points in each direction,in order to achieve the new points root uses Delaunay's triangle interpolation technique. From the plot it is clear that the exclusion is strongest for the gluinos with the lowest masses, grid points up to $(m_{\tilde{q}}, 360\text{ GeV})$ are excluded except for some points close to the diagonal for masses greater than 260 GeV, and some points included in a small area close to $m_{\tilde{q}} = 400$ GeV and $m_{\tilde{g}} = 320$ GeV. The CMS collaboration excluded gluinos in the range 200–280 GeV, while I exclude gluino masses up to 320 GeV more or less, this is not surprising as the squarks also contribute in my study. The fact that the exclusions are best for low gluino masses seems reasonable taking into account that the peak around the gluino is larger than the one around the squark. This can clearly be seen for $m_{\tilde{g}} = 400$ GeV and $m_{\tilde{q}} = 260$ GeV in Fig. 3.4.

There are two main reasons for this, the first one is that at the LHC the gluon-gluon fusion contributes much more at the production level than does fusion between quarks. The cross section for producing two gluinos from gluon–gluon fusion is higher than the cross section for production of $\tilde{q}$ and $\bar{\tilde{q}}$ from gluon–gluon fusion, so the cross section for production of two gluinos is higher than the one for two squarks.

The other argument is that the jet reconstruction is better suited to the gluinos than the squarks. The squarks will either decay into two quarks directly, or four quarks through $\tilde{q} \to q_1\tilde{g}$ and $\tilde{g} \to q_2q_3q_4$. The jet reconstruction of the decaying particles combine 3-jets, the gluino is constrained to decay into three quarks or into a squark and a gluino with the squark decaying into two quarks. So more events from the gluino decay will survive after the reconstruction than what is the case for the decaying squarks. What is prominent with the plot, is that the exclusion is weak in the areas where $m_{\tilde{g}}$ are a little greater than $m_{\tilde{q}}$. This can be explained by the fact that the q from the process $\tilde{g} \to \tilde{q}q$ for small mass differences between squarks and gluinos is so soft that it is difficult to detect.

A similar statistical procedure has been performed in the reproduction of results done in [1]. The signal assumption is

$$F_t(x) = f(x) + nf_s(x). \tag{3.12}$$

$$\chi^2 = \sum_{i=1}^{59} \frac{(O_i - F_t)^2}{\delta_i^2} \tag{3.13}$$

The same analysis as was done in the case with both gluinos and squarks are now done for about 15 gluino masses in the range 200 GeV to 340 GeV, the squark

masses are set to 1 TeV so that their influence are removed. The scaling factor n is obtained for every mass, when this value is smaller than 1, the signal is too large compared to the background, and the gluino mass is excluded at 95% C.L level.

The ratio between NLO and LO cross sections were located in the range 1.7–2.2. A similar analysis is done by the CMS collaboration in the maximum likelihood scheme, here the events are generated by Pythia 6.4 [22].

$m_{\tilde{g}}$ [GeV]	Cross section at 95% C.L [pb]	Cross section at 95% C.L in article [1] [pb]
200	479	383
210	331	273
220	252	214
230	238	200
240	227	184
250	167	132
260	108	88
270	75	72
280	79	73
290	86	79
300	95	86
310	98	89
320	93	87
330	91	82
340	87	80

Table 3.1: Cross section limits for gluino cross section at 95 % C.L.

As one can see in Table 3.1, the 95% cross sections that I have produced in my study and the ones produced by [1] are similar, but there are deviations there that must be accounted for. These deviations may in part be explained by the fact that in the article [1] Pythia is used to generate the events, while I have used Herwig++. In addition it is reasonable to assume that their statistical likelihood analysis is more optimized than mine.

For a given gluino mass the model is excluded at a 95 % C.L when the actual cross section lies above the bounds in Table 3.1 , the cross section bounds I have found are larger than those produced by [1], so my exclusions are more conservative than the ones in the CMS article, hence the analysis with both gluinos and squarks can be trusted to be conservative.

Chapter 4

NLO improved squark decay

The number of jet-triplets coming from the process $\tilde{q} \to q_1 q_2 g$ will be underestimated in Herwig++ because these gluons come from resumed leading logarithmic contributions included in the shower handler. This motivates an analytical study of this decay since the process is crucial for the efficiency of reconstructing squarks in the CMS analysis. I have performed a calculation of this process for hard gluons and compared the result, after similar cuts, to simulation results from Herwig++ for grid points where squark and gluino masses are close to exclusion.

4.1 Width for the gluon radiation process

In this section I calculate the width of a squark decaying into two squarks through a R-parity violating coupling, and the width of the same process with hard gluon radiation. The ratio of the width between the radiation process and the total width will be calculated, the result will be used to estimate the number of jet triplets coming from the process $\tilde{q} \to q_1 q_2 g$, which is compared to the same quantity calculated by Herwig++. From this it is possible to discuss the rate at where jet triplets production on Herwig++ is underestimated, and to quantify how much improvement on the bounds the NLO corrections grants.

The Feynman rules that have been used in the following calculations are listed in appendix A. The Lagrangian terms that are involved in the decay calculation is $L_{UDD} = -\lambda''_{ijk} d^*_k u_i p_R d_j$. The three possible radiation diagrams are shown i Figs. 4.1–4.3 with reading direction for the fermion lines. The index 1 is associated with $\bar{u}$ and the index 2 is associated with $\bar{d}$. The mass of the squark is m, the quark masses will be neglected, the four-momenta of particle 1, 2 and the gluon will be named p_1, p_2 and k respectively. The spin-sum over the total square of the Feynman

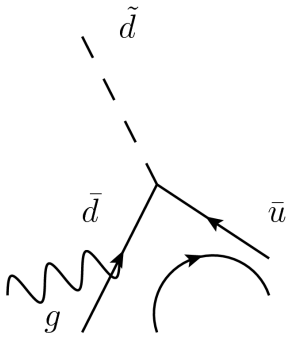

Figure 4.1: Diagram a, $\bar{d}$ emits a gluon

amplitude can be written

$$\begin{aligned}\Sigma_{s1,s2,\mu,\nu}|M|^2 &= \Sigma_{s1,s2,\mu,\nu}|M_a + M_b + M_c|^2 \\ &= \Sigma_{1,2,r,t}|M_a|^2 + |M_b|^2 + |M_c|^2 \\ &\quad +2\Re(M_a^* M_b) + 2\Re(M_b^* M_c) + 2\Re(M_a^* M_c). \end{aligned} \tag{4.1}$$

The formula for the sum over polarization states is given in AppendixB. From the Feynman rules I get

$$M_a = \frac{-ig_s \lambda''_{ijk} \bar{u_2} \gamma^\mu t^a \left(\not{p_2} + \not{k}\right) p_R v_1 \epsilon^r_\mu}{\left(p_2 + k\right)^2}, \tag{4.2}$$

which gives

$$\Sigma_{1,2,r,t}|M_a|^2 = \frac{4g_s^2 |\lambda''_{ijk}|^2 g_{\mu\nu} \mathrm{Tr}\left(p_L \gamma^\mu \gamma^\nu \not{k} \not{p_1}\right) 2p_2 k}{3\left(p_2 + k\right)^4} \tag{4.3}$$

where the sum is taken over spin and polarization for quarks and gluons respectively. The factor 4/3 comes from averaging over colors in the initial state and the sum over final state colors. Evaluating the trace gives

$$\mathrm{Tr}\ (t^a t^a) = 4 \tag{4.4}$$

which leads to

$$\Sigma_{1,2,r,t}|M_a|^2 = \frac{64 g_s^2 |\lambda''_{ijk}|^2 \left(p_1 k\right) \left(p_2 k\right)}{3\left(p_2 + k\right)^4}. \tag{4.5}$$

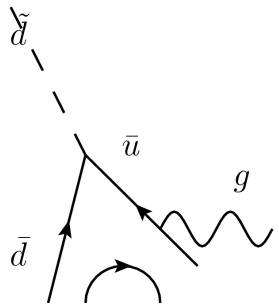

Figure 4.2: Diagram b, $\bar{u}$ emits a gluon

The calculation of $|M_b|^2$, $|M_c|^2$ and the interference terms are similar to the calculation above and will therefore not be done in the same detail. From

$$M_b = \frac{-ig_s\lambda''_{ijk}\bar{u_2}p_R\left(\not{p_1}+\not{k}\right)\gamma^\mu t^a v_1\epsilon^r_\mu}{\left(p_1+k\right)^2}, \tag{4.6}$$

I get

$$\Sigma_{1,2,r,t}|M_b|^2 = \frac{64g_s^2|\lambda''_{ijk}|^2\left(p_2k\right)\left(p_1k\right)}{3\left(p_1+k\right)^4}, \tag{4.7}$$

and from

$$M_c = \frac{ig_s\lambda''_{ijk}\bar{u_2}p_R v_1\left(p_1+p_2+k\right)\epsilon^r_\mu t^a}{\left(p_1+p_2\right)^2-m^2}, \tag{4.8}$$

I get

$$\Sigma_{1,2,r,t}|M_c|^2 = \frac{32g_s^2|\lambda''_{ijk}|^2\left(p_1p_2\right)\left(\left(p_1k\right)+\left(p_2k\right)+2\left(p_1p_2\right)\right)}{3\left(\left(p_1+p_2\right)^2-m^2\right)^2}. \tag{4.9}$$

The interference terms are

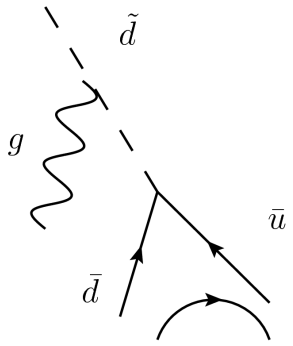

Figure 4.3: Diagram c, $\tilde{d}$ emits a gluon

$$\Sigma_{1,2,r,t} 2\Re(M_a M_c^*) = \frac{-32 g_s^2 |\lambda''_{ijk}|^2 (p_1 p_2)(k p_1)}{3\left((p_1+p_2)^2 - m^2\right)(p_1+k)^2}, \tag{4.10}$$

$$\Sigma_{1,2,r,t} 2\Re(M_a M_b^*) = \frac{-64 g_s^2 |\lambda''_{ijk}|^2 (p_2 k)(p_1 k)}{3(p_1+k)^2 (p_2+k)^2}, \tag{4.11}$$

$$\Sigma_{1,2,r,t} 2\Re(M_c M_b^*) = \frac{-32 g_s^2 |\lambda''_{ijk}|^2 (p_1 p_2)(k p_2)}{3\left((p_1+p_2)^2 - m^2\right)(p_2+k)^2}. \tag{4.12}$$

The total amplitude is then

$$\begin{aligned}
\Sigma_{1,2,r,t}|M|^2 = {} & \frac{64 g_s^2 |\lambda''_{ijk}|^2 (p_1 k)(p_2 k)}{3(p_2+k)^4} + \frac{64 g_s^2 |\lambda''_{ijk}|^2 (p_2 k)(p_1 k)}{3(p_1+k)^4} \\
& + \frac{32 g_s^2 |\lambda''_{ijk}|^2 (p_1 p_2)\left((p_1 k)+(p_2 k)+2(p_1 p_2)\right)}{3\left((p_1+p_2)^2 - m^2\right)^2} \\
& - \frac{32 g_s^2 |\lambda''_{ijk}|^2 (p_1 p_2)(k p_1)}{3\left((p_1+p_2)^2 - m^2\right)(p_1+k)^2} \\
& - \frac{64 g_s^2 |\lambda''_{ijk}|^2 (p_2 k)(p_1 k)}{3(p_1+k)^2 (p_2+k)^2} \\
& - \frac{32 g_s^2 |\lambda''_{ijk}|^2 (p_1 p_2)(k p_2)}{3\left((p_1+p_2)^2 - m^2\right)(p_2+k)^2}.
\end{aligned} \tag{4.13}$$

When Dalitz kinematics is used, the differential width for a three-body decay can be written

$$d\Gamma = \frac{|\bar{M}|^2 dm_{12}^2 dm_{23}^2}{(2\pi)^3 32m^3}. \tag{4.14}$$

The variables m_{12} and m_{23} are the invariant mass between particles 1 and 2 and 2 and 3 respectively. The invariant mass between two mass-less particles can be written as

$$m_{ij}^2 = 2p_i p_j = 2E_i E_j \left(1 - \cos\theta_{ij}\right). \tag{4.15}$$

I denote the invariant mass between the two quarks by m_{12}, the invariant mass between the gluon and quark 1 is m_{1k} and the invariant mass between the gluon and quark 2 is m_{12}. In the case where the quarks have zero mass the following relation is satisfied

$$m^2 = m_{12}^2 + m_{1k}^2 + m_{2k}^2. \tag{4.16}$$

From these kinematical equations I get the following expression for the differential decay rate

$$d\Gamma_3 = \frac{g_s^2 |\lambda''_{ijk}|^2 dm_{1k}^2 dm_{2k}^2 A\left(m_{1k}^2, m_{2k}^2\right)}{(2\pi)^3 6m^3}. \tag{4.17}$$

Where the dimensionless mass function A is defined as

$$\begin{aligned} A\left(m_{1k}^2, m_{2k}^2\right) &= \frac{m_{1k}^2}{m_{2k}^2} + \frac{m_{2k}^2}{m_{1k}^2} + \frac{m^2\left(m^2 - m_{1k}^2 - m_{2k}^2\right)}{\left(m_{1k}^2 + m_{2k}^2\right)^2} \\ &\quad + \frac{m^2 - m_{1k}^2 - m_{2k}^2}{2\left(m_{1k}^2 + m_{2k}^2\right)} - 1. \end{aligned} \tag{4.18}$$

One can see from Eq. (4.15) that the expression above diverges both when the energy goes to zero and when the angle between the particles goes to zero. The divergences that appear when the energy goes to zero are called soft and those which appear when the angle goes to zero are called collinear. In order to cope with these divergences I introduce a cut in the invariant mass. The alternative is to calculate the NLO loop diagrams that regulate the divergence, however, the experiments have a limited resolution on the gluon jets that this cut emulates, so this is sufficient for looking at the radiation processes.

I start by integrating out the variable m_{2k} with $m_{2min}^2 = m_{min}^2$ as the lower limit and $m^2 - m_{1k}^2$ as the upper limit. The upper limit is the standard boundary of a

Dalitz plot, found in the PDG booklet [15], demanding that Eq. (4.16) is fulfilled I get

$$d\Gamma_3 = dm_{1k}^2 \int_{m_{min}^2}^{m^2-m_{1k}^2} \frac{g_s^2 |\lambda_{ijk}^{''}|^2 dm_{2k}^2 A\left(m_{1k}^2, m_{2k}^2\right)}{(2\pi)^3 6m^3}. \tag{4.19}$$

This gives

$$d\Gamma_3 \;=\; dm_{1k}^2 \frac{\alpha_s |\lambda_{112}^{''}|^2}{12\pi^2 m^3} K\left(m_{1k}^2\right), \tag{4.20}$$

where the mass function K is defined as

$$\begin{aligned} K\left(m_{1k}^2\right) \;\equiv\; & m_{1k}^2 \log \frac{m^2 - m_{1k}^2}{m_{min}^2} + \frac{1}{2m_{1k}^2}\left(\left(m^2 - m_{1k}^2\right)^2 - m_{min}^4\right) \\ & -m^2 + \frac{m^4}{\left(m_{1k}^2 + m_{min}^2\right)} - \frac{m^2}{2} \log \frac{m^2}{\left(m_{1k}^2 + m_{min}^2\right)} \\ & -\frac{3}{2}\left(\left(m^2 - m_{1k}^2\right) - m_{min}^2\right). \end{aligned} \tag{4.21}$$

Then we finally integrate out m_{1k} with $m_{1min}^2 = m_{min}^2$ as lower limit and $m^2 - m_{1min}^2$ as upper limit and obtain the total width:

$$\Gamma_3 = \frac{\alpha_s |\lambda_{ijk}^{''}|^2}{12\pi^2 m^3} B\left(m, m_{min}\right) \tag{4.22}$$

Where

$$B\left(m, m_{min}\right) \;=\; \int_{m_{min}^2}^{m^2-m_{min}^2} dm_{1k}^2 K\left(m_{1k}^2\right). \tag{4.23}$$

$$\begin{aligned} B\left(m, m_{min}\right) = & \, m^4 \log\left(\frac{m^2 - m_{min}^2}{m_{min}^2}\right) \\ & - \frac{m_{min}^4}{2} \log\left(\frac{m^2 - m_{min}^2}{m_{min}^2}\right) \\ & - m_{min}^2 m^2 \log\left(\frac{2m_{min}^2}{m^2}\right) \\ & + m^4 \log\left(\frac{m^2}{2m_{min}^2}\right) - 4m^4 \\ & - 3m_{min}^4 + \frac{37}{4} m^2 m_{min}^2 \end{aligned} \tag{4.24}$$

When $m_{min} << m$ the terms that contain m_{min}^4 and $m_{min}^2 m^2$ can be neglected. The terms $-m_{min}^2 m^2 \log\left(\frac{2m_{min}^2}{m^2}\right)$ and $-\frac{m_{min}^4}{2}\log\left(\frac{m^2-m_{min}^2}{m_{min}^2}\right)$ are investigated with L'Hospital's rule and it approaches zero as m_{min}^2 goes to zero. So one gets

$$B\left(m, m_{min}\right) \simeq m^4 \log\left(\frac{m^2 - m_{min}^2}{m_{min}^2}\right) + m^4 \log\left(\frac{m^2}{2m_{min}^2}\right) - 4m^4. \tag{4.25}$$

I plot $\Gamma_3/|\lambda''_{ijk}|^2$ in Fig. 4.4 as a function of the choice of cut on invariant mass m_{min}^2 for $m_{\tilde{q}} = 180$ GeV. This shows that the width only varies much when the cut is close to zero due to the divergences then, so for appropriate cuts Γ_3 stays relatively constant, which implies that it is not necessary to calculate Γ_3 for more than one value of m_{min} when I later compare to similar cuts in the Monte Carlo simulation.

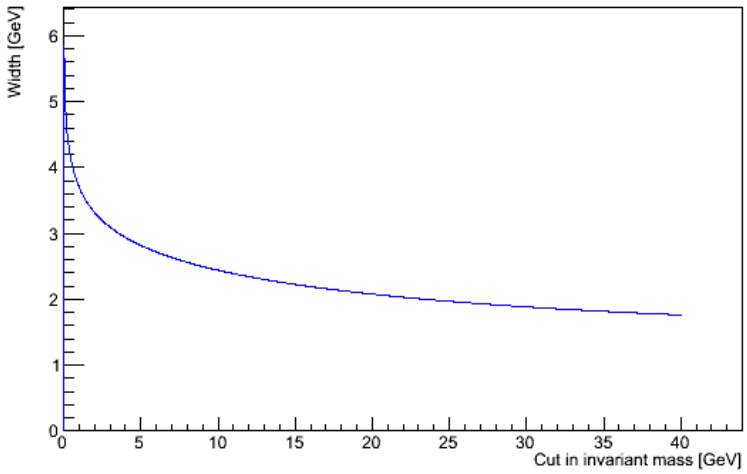

Figure 4.4: $\frac{\Gamma_3}{|\lambda''_{ijk}|^2}$ plotted against m_{min} for $m_{\tilde{q}} = 180$GeV

I set the cut at $m_{min}^2 = 0.01m^2$ as done in [23] and get

$$\Gamma_3 = \frac{4.5m\alpha_s|\lambda''_{ijk}|^2}{12\pi^2}. \tag{4.26}$$

The value that is interesting in this study is the ratio between the width of the radiation process I have studied and the width of a squark decaying into two quarks. The Feynman amplitude for the tree level diagram shown in Fig. 4.5 is

$$M = -i\lambda''_{ijk} v_1 P_R \bar{u}_2. \tag{4.27}$$

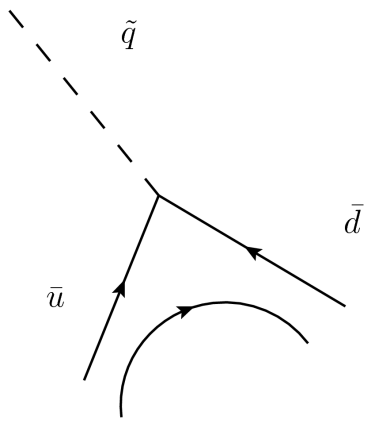

Figure 4.5: Squark decaying into two quarks

This gives the spin averaged squared amplitude

$$\Sigma_{1,2}|M|^2 = 2|\lambda''_{ijk}|^2 p_1 p_2 = |\lambda''_{ijk}|^2 m^2. \tag{4.28}$$

In the rest frame of the decaying particle the width is given as:

$$\Gamma_2 = \frac{|\vec{p}||M|^2}{8\pi m} \tag{4.29}$$

When the two particles in the final state are mass-less $|\vec{p}| = m/2$. This gives a width for the two body decay of

$$\Gamma_2 = \frac{|\lambda''_{ijk}|^2 m}{16\pi}. \tag{4.30}$$

Thus the ratio that will be used to estimate the number of jet triplets coming from the process $\tilde{q} \to q_1 q_2 g$ is

$$\frac{\Gamma_3}{\Gamma_2 + \Gamma_3} = \frac{17.86\alpha_s}{3\pi + 17.86\alpha_s} \tag{4.31}$$

4.2 Analysis of scenarios close to exclusion

As mentioned in the beginning of this chapter, the grid points of squark and gluino masses that are close to exclusion will be further investigated. I call the number of jet triplets coming from the squark decay which is generated by Herwig++ for E. This number can be estimated by taking the area of the peak above the combinatorial background shown in Fig. 4.6. This is done by finding a linear fit to the

combinatorial background and then finding the area in between this linear function and the Gaussian fit function of the peak described in chapter 3. The trapezoidal method has been used in order to obtain this integral, the integration limits are the points where the Gaussian and the linear fit intercept. For the concerned grid points $m_{\tilde{g}} > m_{\tilde{q}}$, this means that jet triplet states that are produced by the squarks comes from the process $\tilde{q} \rightarrow q_1 q_2 g$.

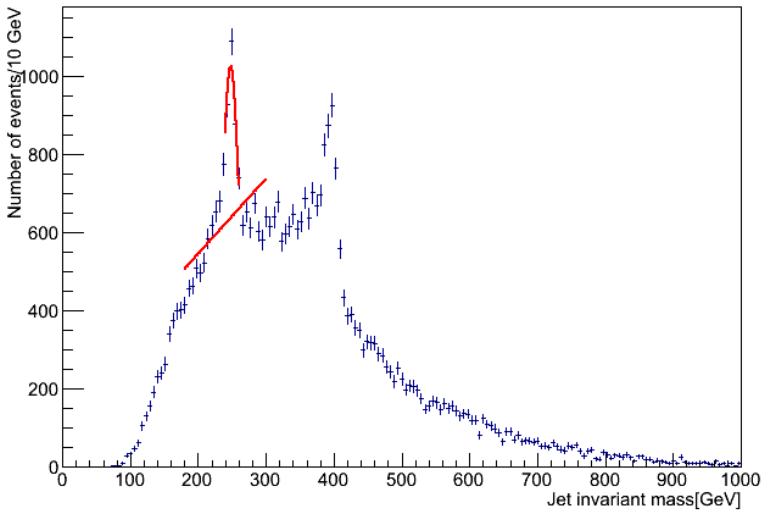

Figure 4.6: Plot of triplet invariant mass where the estimate of the area E is shown for $m_{\tilde{q}} = 240$ GeV and $m_{\tilde{g}} = 400$ GeV.

The number of such events can also be estimated analytically. The analytical width of the radiation process was calculated with a cut in invariant mass, while the cuts in the numerical simulations are taken in transverse momentum and pseudorapidity when reconstructing the jets. The process of translating these cuts into a cut in invariant mass is difficult and can only be done on an event by event basis, because the system where the squark is at rest is achieved by Lorentz boosting the lab system two times,once for the hard scatter and once for the longitudinal boost of interacting gluons and quarks. However, it turns out this is not necessary because Γ_3 is relatively insensitive to m^2_{min}.

One can see from the plot for $m_{\tilde{g}} = 180$ GeV in Fig. 4.4 that Γ_3 varies slowly when m_{min} is not close to zero. One might also wonder whether the transverse energy of the gluon with this invariant mass cut is large enough to be picked up by the selection criteria used in the simulation. When the jets originated from the

two quarks are separated from each other, it can be argued from $m_{min}^2 > km^2$, $m_{12}^2 \approx 2E_{1T}E_{2T}\left(1-\cos\theta_{12}\right)$ and $m^2 = m_{12}^2 + m_{1k}^2 + m_{2k}^2$ that E_{1T} and E_{2T} cannot exceed a certain value. Further, one can use that $m_{1k}^2 \approx 2E_{1T}E_{kT}\left(1-\cos\theta_{1k}\right)$ to obtain a lower boundary on E_{kT}.

With expressions for both Γ_2 and Γ_3 at hand, one can obtain a more accurate estimate for the value E, this quantity will be called A. It is given by

$$A = \frac{2N\Gamma_3\epsilon}{\Gamma_2 + \Gamma_3}. \tag{4.32}$$

Here N is the total number of events generated by the Monte Carlo simulation and ϵ is the efficiency for reconstructing a squark decaying into three well separated partons. Given that the kinematical cuts are the same for the gluino and the squark one can do the estimate $\epsilon = B/2N$, where B is the area of the peak around the gluino mass when the mass of the gluino and the squarks are swapped. The value of α_s runs so slowly, that one can use the value $\alpha_s\left(\mu\right) \approx \alpha_s\left(m_Z\right) \approx 0.11$, where μ is the energy scale of the interaction.

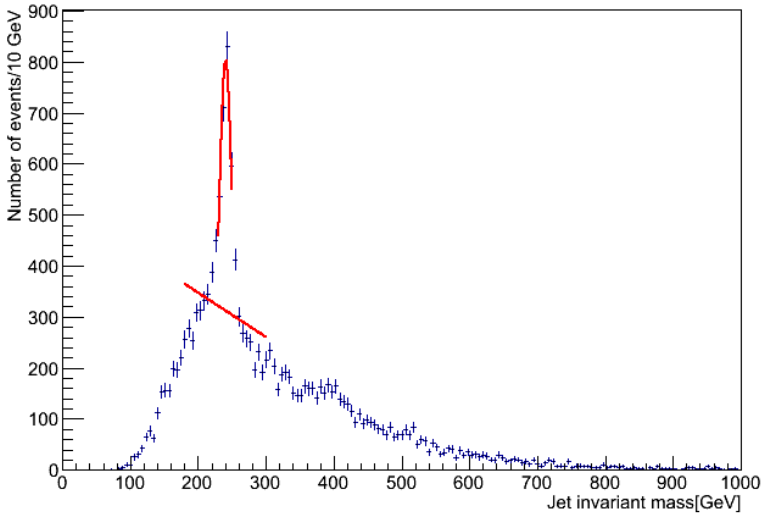

Figure 4.7: Plot of triplet invariant mass where the estimate of the area B is shown for a model with $m_{\tilde{q}} = 400$ GeV and $m_{\tilde{g}} = 240$ GeV.

The quantity B is in the same way as E obtained by integrating out the area between the linear and the Gaussian fit. The expected number A of jet triplets events coming from squark decay and gluon emission can be found once B is extracted. As

$m_{\tilde{g}}$ [GeV]	$m_{\tilde{q}}$ [GeV]	B	E	A	A/E	$\sigma_{A/E}$
400	160	6181	356	1062	2.98	0.18
400	180	5762	364	990	2.72	0.17
400	200	5755	456	989	2.17	0.12
400	220	5727	482	983	2.04	0.12
400	240	4601	387	791	2.04	0.13
400	260	3091	256	512	2.07	0.15
400	280	2762	237	473	1.99	0.15
400	300	2496	229	429	1.87	0.15
400	320	1755	184	301	1.64	0.15
400	340	1678	174	288	1.66	0.16
400	360	1001	108	172	1.59	0.19

Table 4.1: Effective number of events from the radiation processes using a simulation of $N = 500000$ events, the quantities in this table are defined in the text.

one can see from Table 4.1 there is a clear tendency that the number of expected jet triplets is greater than the same quantity calculated in Herwig++.

According to this result it should be possible to obtain stronger limits on the masses by incorporating the NLO decay rate in the simulation. From Table 4.1 one can also observe that the ratio A/E is decreasing when the squark mass is increasing, the squark is produced with low p_T on average so a lot of the energy in the gluons is originated from the mass of the squark. When the squark mass is small the energy that goes into the gluons will be even more underestimated by the shower calculation in Herwig++, which leads to the behaviour shown in Fig. 4.1. As one can observe in Fig. 3.8 the points were $m_{\tilde{g}} = 400$ GeV and $320 > m_{\tilde{q}} > 200$ GeV are the points closest to exclusion. For these grid points the ratio A/E in Table 4.1 are between 1.8–2.2 and the scaling factor at 95 % C.L vary in the range between 1.1 and 1.5. The number of events in the peak around the squark are larger than the number of events in the peak around the gluino mass for these masses, so it is reasonable to believe that a numerical study with NLO improvements would exclude these points at a 95 % confidence level.

Chapter 5

Conclusion

I have simulated proton–proton collisions with production of gluinos and squarks. The lightest one of them was assumed to be the NLSP, with a possible gravitino or axino LSP, and could only decay through a R-Parity violating channel due to the suppression of the R-parity conserving decay of the NLSP to the LSP. The products of these decays were mainly two or three colored particles that would shower and hadronize before reaching the detector, which motivated the search for jet triplets resonances.

I defined a grid of squark and gluino masses in the range 160–420 GeV. The simulation was done for all of these points, with the number of events plotted against the jet triplet invariant mass following an analysis published by the CMS collaboration [1]. Gaussian curves were fitted to the peaks around the gluino and squark masses. These fit points were used in a $\Delta\chi^2$ analysis where the result was a plot of the limit on the scaling of the against squark and gluino cross section at 95% confidence level. Masses are excluded when the corresponding scaling factor is below 1. It turned out I could exclude up to about 360–380 GeV in gluino mass, except for points close to the diagonal, when masses were greater than 260 GeV and some points included in a small area close to $m_{\tilde{q}} = 400$ GeV and $m_{\tilde{g}} = 320$ GeV. The CMS article [1] excludes gluino masses in the range 200–280 GeV, while my study excludes gluino masses up to 320 more or less, which is reasonable because of contributions from the squarks.

I argued that the number of events in the peak around the squark mass was underestimated, a calculation of this number in the NLO scheme was performed, this number was compared to the ones I got from the simulation for grid points where $m_{\tilde{g}} = 400$ GeV and $m_{\tilde{q}} < 380$ GeV. The points where $m_{\tilde{g}} = 400$ GeV and $320 > m_{\tilde{q}} > 200$ GeV were most interesting to discuss because these grid points had enhancements in the number of events that could balance the worse limits on the scaling factor. For these points the values A/E in Table 4.1 were in the range 1.8–2.2 and the limit on the scaling factor varied in the range 1.1–1.5. In addition,

the peak around the squark are larger than the peak around the gluino mass for these grid points, so it is reasonable to believe that a numerical study with the NLO improvements included would exclude these points at a 95 % confidence level as well. This analysis can be extended to also involve proton–proton collisions at 14 TeV if LHC results are published. However, one has to be aware of that backgrounds and selection criteria will be different from what was used in this study.

Appendix A

Feynman rules

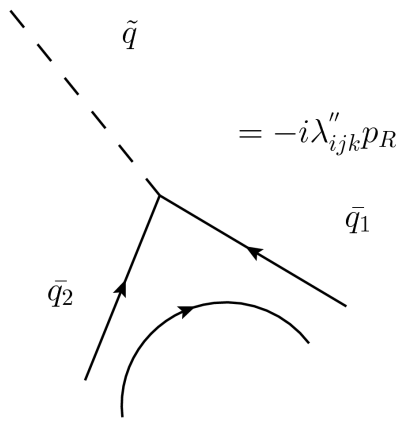

Figure A.1: R-parity violating vertex between a squark and two quarks from the $\bar{U}\bar{D}\bar{D}$ operator.

The vertex in Fig. A.1 is $-\lambda''_{ijk} P_R$ The P_R is consistent with a clockwise reading direction. The squark is a spin-less object so there are no spinor related to it.

The fermion propagator is

$$S(p) = \frac{\not{p} + m}{p^2 - m^2 + i\epsilon} \tag{A.1}$$

where m is the mass of the propagator and p is its four-momentum. The spinor of an incoming quark line is

$$\xrightarrow[\rightarrow]{} = \bar{u_2}(p_2, s_2)\,. \tag{A.2}$$

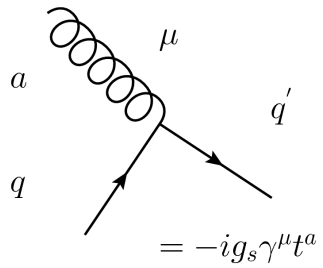

Figure A.2: The vertex between a gluon and two quarks

The spinor of outgoing quark number 1 is

$$\overleftarrow{\underrightarrow{}} = v_1(p_1, s_1). \tag{A.3}$$

The arrow above is the fermion flow and the arrow below is the reading direction. The sum over polarization states for massless gluons are

$$\Sigma_{r,t}\epsilon^r_\mu \epsilon^s_\nu = -g_{\mu\nu}. \tag{A.4}$$

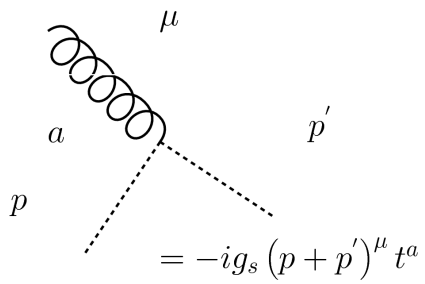

Figure A.3: The vertex between a gluon and two squarks

Appendix B

Formulae

The metric tensor used in particle physics is:

$$g_{\mu\nu} = \begin{pmatrix} 1 & 0 & 0 & 0 \\ 0 & -1 & 0 & 0 \\ 0 & 0 & -1 & 0 \\ 0 & 0 & 0 & -1 \end{pmatrix}$$

.

A Dirac spinor ϕ can be written:

$$\phi_a = \begin{pmatrix} \chi_A \\ \psi_{\dot{A}} \end{pmatrix}$$

, where χ_A and $\phi_{\dot{A}}$ are left and right handed Weyl-spinors respectively. Products of weyl spinors ψ and χ can be defined as

$$\bar{\psi}\bar{\chi} = \bar{\psi}_{\dot{A}}\bar{\chi}^{\dot{A}} = \epsilon_{\dot{A}\dot{B}}\bar{\psi}^{\dot{B}}\chi^{\dot{A}}. \tag{B.1}$$

$$\psi\chi = \psi^A\chi_A = \epsilon^{AB}\psi_B\chi_A \tag{B.2}$$

In particular:

$$\psi^2 = \psi^A\psi_A = \epsilon^{AB}\psi_B\psi_A = \psi_2\psi_1 - \psi_1\psi_2 = -2\psi_1\psi_2, \tag{B.3}$$

$$\bar{\psi}^2 = \bar{\psi}_{\dot{A}}\bar{\psi}^{\dot{A}} = \epsilon_{\dot{A}\dot{B}}\bar{\psi}^{\dot{B}}\psi^{\dot{A}} = 2\psi_{\dot{1}}\psi_{\dot{2}} \tag{B.4}$$

The lowering operator used here is expressed as

$$\epsilon_{AB} = \epsilon_{\dot{A}\dot{B}} = \begin{pmatrix} 0 & -1 \\ 1 & 0 \end{pmatrix}$$

, while the raising operator is given by:

$$\epsilon^{AB} = \epsilon^{\dot{A}\dot{B}} = \begin{pmatrix} 0 & 1 \\ -1 & 0 \end{pmatrix}$$

.

The definition of the commutator is

$$[A, B] = AB - BA. \tag{B.5}$$

The anti-commutator is defined by

$$\{A, B\} = AB + BA. \tag{B.6}$$

The Pauli matrices are:

$$\sigma_1 = \begin{pmatrix} 0 & 1 \\ 1 & 0 \end{pmatrix}$$

$$\sigma_2 = \begin{pmatrix} 0 & -i \\ i & 0 \end{pmatrix}$$

$$\sigma_3 = \begin{pmatrix} 1 & 0 \\ 0 & -1 \end{pmatrix}$$

The eight Gell-Mann matrices of $SU(3)$ are

$$\lambda_1 = \begin{pmatrix} 0 & 1 & 0 \\ 1 & 0 & 0 \\ 0 & 0 & 0 \end{pmatrix}$$

,

$$\lambda_2 = \begin{pmatrix} 0 & -i & 0 \\ i & 0 & 0 \\ 0 & 0 & 0 \end{pmatrix}$$

,

$$\lambda_3 = \begin{pmatrix} 1 & 0 & 0 \\ 0 & -1 & 0 \\ 0 & 0 & 0 \end{pmatrix}$$

,

$$\lambda_4 = \begin{pmatrix} 0 & 0 & 1 \\ 0 & 0 & 0 \\ 1 & 0 & 0 \end{pmatrix}$$

,

$$\lambda_5 = \begin{pmatrix} 0 & 0 & -i \\ 0 & 0 & 0 \\ i & 0 & 0 \end{pmatrix}$$

,

$$\lambda_6 = \begin{pmatrix} 0 & 0 & 0 \\ 0 & 0 & 1 \\ 0 & 1 & 0 \end{pmatrix}$$

,

$$\lambda_7 = \begin{pmatrix} 0 & 0 & 0 \\ 0 & 0 & -i \\ 0 & i & 0 \end{pmatrix}$$

,

$$\lambda_8 = \frac{1}{\sqrt{3}} \begin{pmatrix} 1 & 0 & 0 \\ 0 & 1 & 0 \\ 0 & 0 & -2 \end{pmatrix}$$

.

The generators are

$$t_a = \frac{\lambda_a}{2}. \tag{B.7}$$

From this one gets Eq. (4.4) The Dynkin index of a representation is given by

$$\mathrm{Tr}\left[t_a, t_b\right] = T\left(R\right)\delta_{ab}. \tag{B.8}$$

The γ matrices satisfy the following anti-commutation relation

$$\{\gamma^\mu, \gamma^\nu\} = 2g^{\mu\nu}. \tag{B.9}$$

Where the Feynman slash notation is

$$\not{a} = \gamma^\mu a_\mu. \tag{B.10}$$

It is useful to define the product of gamma matrices

$$\gamma^5 = i\gamma^0\gamma^1\gamma^2\gamma^3. \tag{B.11}$$

The operators left and right handed projection operators are

$$p_L = \frac{1}{2}\left(1 - \gamma^5\right), \tag{B.12}$$

$$p_R = \frac{1}{2}\left(1 + \gamma^5\right). \tag{B.13}$$

The trace of any product of an odd number of γ^μ is zero. Furthermore,

$$\mathrm{Tr}\ \left(\gamma^\mu\gamma^\nu\right) = 4g^{\mu\nu}, \tag{B.14}$$

$$\mathrm{Tr}\ \left(\gamma^\mu\gamma^\nu\gamma^\rho\gamma^\sigma\right) = 4\left(g^{\mu\nu}g^{\rho\sigma} - g^{\mu\rho}g^{\nu\sigma} + g^{\mu\sigma}g^{\nu\rho}\right), \tag{B.15}$$

$$\mathrm{Tr}\ \left(\gamma^5\right) = \mathrm{Tr}\ \left(\gamma^\mu\gamma^\nu\gamma^5\right) = 0. \tag{B.16}$$

Spinor contractions can be rewritten as traces by using

$$\bar{u}Nu = \text{Tr } (Nu\bar{u}) \tag{B.17}$$

where N are some product of gamma matrices. The Dirac spinors u and v satisfy the completeness relations

$$\Sigma_s u\left(s,p\right)\bar{u}\left(s,p\right) = \not{p} + m, \tag{B.18}$$

$$\Sigma_s v\left(s,p\right)\bar{v}\left(s,p\right) = \not{p} - m \tag{B.19}$$

where m and p is the mass and the four-momentum of the particle respectively.

Appendix C

Codes

C.0.1 Code used to obtain jet information

This program is linked to Herwig++ and produces a ROOT file which contains information abaout the jets in the final state for all the generated events. Root [24] has also been used for plotting.

```
//This program is based on the rootsimple.cc analysis file in the
    Herwig++ distribution.

#include "TTree.h"
#include "TFile.h"
#include "TStyle.h"
#include "TH1F.h"

#include <cmath>
#include <fstream>

#include "col.h"
#include "ThePEG/Repository/EventGenerator.h"
#include "ThePEG/EventRecord/Particle.h"
#include "ThePEG/Vectors/ThreeVector.h"
#include "ThePEG/EventRecord/Event.h"
#include "ThePEG/PDT/EnumParticles.h"
#include "ThePEG/Interface/ClassDocumentation.h"
#include "ThePEG/Persistency/PersistentOStream.h"
#include "ThePEG/Persistency/PersistentIStream.h"
#include "fastjet/ClusterSequence.hh"
#include <iostream>
using namespace fastjet;
using namespace std;
using namespace MyName;

```

```
27 //the following function is called for each event
   void col::analyze(tEventPtr event, long, int, int) {
29
     //the 4-momentum for each particle
31   Lorentz5Momentum p5;
     //get the final-state particles in the event
33   tPVector finalstate = event->getFinalState();
     vector <PseudoJet> particles;
35   //loop over all the final state particles
     for(int iii = 0; iii < finalstate.size(); iii++) {
37     //put the momentum of the current particle in the 4-vector
       p5=finalstate[iii]->momentum();
39     //fill in the objects array with the necessary components
       //objects[0][iii] = p5.e()/GeV;
41     if(abs(finalstate[iii]->id()) !=12 && abs(finalstate[iii]->id())
          !=14 && abs(finalstate[iii]->id()) !=16 && abs(finalstate[iii
          ]->eta()) < 5.0 ){
         particles.push_back(PseudoJet(p5.x()/GeV,p5.y()/GeV,p5.z()/GeV,
            p5.e()/GeV));
43     }
     }
45
47
     double R = 0.5;
49   JetDefinition jet_def(antikt_algorithm, R);
     //run the clustering, extract the jets
51   ClusterSequence cs(particles, jet_def);
     vector<PseudoJet> jets = sorted_by_pt(cs.inclusive_jets());
53   //vector<fastjet::PseudoJet> sorted_by_pt(const vector<fastjet::
        PseudoJet> & jets) ;
     numparticles = 0;
55   // cout<<jets[0].px()<<endl;

57   for(int j = 0;j<jets.size();j++){
       if(jets[j].perp()>=20){numparticles+=1;}
59     if(jets[j].perp() < 20) break;
       objects[0][j] = jets[j].e();
61     objects[1][j] = jets[j].px();
       objects[2][j] = jets[j].py();
63     objects[3][j] = jets[j].pz();
       objects[4][j] = jets[j].perp();
65     objects[5][j] = jets[j].eta();
     }
67
69
71
```

```
  Crossection = generator()->integratedXSec() ;
  objects[5][14] = Crossection*(pow(10.0,31.0));
  Data->Fill();

}


//put the data in the ROOT tree
//this is the initalization function, put any new branches you want to
    create here, remember to declare them in the rootsimple.h file as
    well
int col::prepareroottree() {
  std::cout << "Preparing Root Tree" << endl;
  dat = new TFile("hpp355.root", "RECREATE");
  Data = new TTree ("Data", "Data Tree");
  Data->Branch("objects", &objects, "objects[6][15]/D");
  Data->Branch("numparticles", &numparticles, "numparticles/I");
  return 1;
}

//write the root tree to a file (hpp.root by default)
int col::writeroottree() {
  Data->GetCurrentFile();
  Data->Write();
  dat->Close();
  // cout<<1000000<<endl;
  cout << "A root tree has been written to a file" << endl;
  return 1;
}


NoPIOClassDescription<col> col::initcol;
// Definition of the static class description member.

void col::Init() {
  // std::cout << "ROOT SimpleAnalysis v1.00 (110210)" << endl;



  //static ClassDocumentation<rootsimple> documentation
  //("The rootsimple class prints 4-moment and IDs of all"
  // " final-state particles");

}

void col::dofinish() {
  AnalysisHandler::dofinish();
  writeroottree ();
  cout << "Total cross section = " << objects[5][14] << "   " <<
```

```
    generator()->integratedXSecErr() << endl;
}
```

/mn/felt/u8/haavass/col/col.cc

C.0.2 Code used to obtain fit parameters

This program reads in root files and produces text files which containes cross sections and the parameters of the fit to the excitations in the events plot.

```
//This program is based on the ratt.cpp analysis file in the Herwig++
    distribution.
#include <TROOT.h>
#include <TChain.h>
#include <TFile.h>
#include <TTree.h>
#include <TH1.h>
#include <TH2.h>
#include <TGraph.h>
#include <TCanvas.h>
#include <TRandom.h>
#include <TRandom3.h>
#include <TLorentzVector.h>
#include <TString.h>
#include "TopHist.h"
//A few standard headers
#include <iostream>
#include <fstream>
#include <utility>
#include <cmath>
#include <string>
#include <time.h>
#include <vector>
#include "TFitResult.h"
#include "TF1.h"
#include <cstdlib>
#include <stdio.h>
#include <math.h>
using namespace std;

int ipow(int a, int b){
  int c=1;
  while (b>0){
    if (b%2) c*=a;
    a*=a;
    b/=2;
  }
  return c;
```

```
}
int imult(int a, int b){
  int c=0;
  while (b>0){
    if (b%2)c+=a;
    a*=2;
    b/=2;
  }
  return c;
}

void analysis(char* rootfile1);
void analysis_once(char* rootfile1);
double sqr(double x);

//declare a few global variables, used to take the branches
double objects[6][15];
int numparticles = 0;
//double Crossection ;

//cuts


//the main function
int main(int argc, char *argv[]){



  char* infile = "";
  if(argv[1]) { infile = argv[1];}
  //else { cout << "Use: ./ratt [input] [output]" << endl; exit(1); }

  //call the analysis code
   analysis(infile);
  //cout << "done! wrote topdrawer output in " << outfile << endl;


}

void analysis(char* rootfile1) {


  FILE * pFile;
  pFile = fopen (rootfile1,"r");
  char str[20];


 for(int i=0; i< 1; i++){
    fscanf (pFile, "%s", str);
```

```
87      cout << str << endl;
        analysis_once(str);
89
91    }

93    fclose(pFile);
  }
95

97  void analysis_once(char* rootfile1) {

99    cout << "analysing " << rootfile1 << endl;
      TFile * f = new TFile("plots.root","recreate");
101   //set the entries of the objects array to 0;

103   // String surgery on file name
      TString * s = new TString(rootfile1);
105   TString * s1 = new TString(rootfile1);
      int iMass;
107   int iMass2;
      s->Remove(0,3);
109   s->Remove(3,4);
      iMass = s->Atoi();
111   s1->Remove(0,6);
      s1->Remove(6,4);
113   iMass2 = s1->Atoi();
      //cout<<"Mass"<<iMass<<endl;
115
  for(int fff = 0; fff < 6; fff++) { for(int aaa = 0; aaa < 15; aaa++) {
       objects[fff][aaa] = 0; }}
117   TChain t("Data");
      //add the rootfile given in the command line
119   t.Add(rootfile1);

121   //set the addresses of the ROOT branches
      t.SetBranchAddress("objects",&objects);
123   t.SetBranchAddress("numparticles", &numparticles);
      // t.SetBranchAddress("Crossection",&Crossection);
125



127
      //get the event numbers
129   int EventNumber = 0;
      EventNumber = int(t.GetEntries());
131   cout << "contains: " << EventNumber << " events " << endl;

133   TH1F* histo;
      histo = new TH1F("",  " ", 175, 0,1000);
```

```
135   TH1F* histo3;
      histo3 = new TH1F("test", "Plot ", 1000, 0, 1000);
137   TH1F* histo2;
      histo2 = new TH1F("test", "Plot ", 1000, 0, 1000);
139   //TH1F* histo4;
      //histo4 = new TH1F("test1", "Plot ", 100, 0,1000);
141
      //int m = 0;
143   //loop over events
      for(int ii = 0; ii < EventNumber; ii++) {
145
        if(ii%100 == 0) { cout << "Event number: " << ii << "\r" << flush;
            }
147     //cout << ii << endl;
        t.GetEntry(ii);//get entries from the root file
149     //m+=numparticles;
        double Ma[numparticles][numparticles][numparticles];
151     double a;
        double b;
153


155
        b = 0;
157     for(int j = 0;j<numparticles;j++){
          if(numparticles >=6){
159     b+= objects[4][j];
      for(int k = j+1;k<numparticles;k++){
161       for(int l = k+1;l<numparticles;l++){
            Ma[l][k][j] =  sqrt(pow((objects[0][j]+objects[0][k]+objects
                [0][l]),2)-pow((objects[1][j]+objects[1][k]+objects[1][l])
                ,2)-pow((objects[2][j]+objects[2][k]+objects[2][l]),2)-pow((
                objects[3][j]+objects[3][k]+objects[3][l]),2));
163         a = abs(objects[4][j])+abs(objects[4][k])+abs(objects[4][l]);
            if(abs(objects[5][j])<3 && abs(objects[5][k]) <3 &&  abs(
                objects[5][l])<3){
165           if( abs(objects[4][j])>45 && abs(objects[4][k])>45&& abs(
                  objects[4][l])>45){
        if(Ma[l][k][j]<a-130&&b>425 ){
167       histo->Fill(Ma[l][k][j]);

169     }
      }
171       }
        }
173   }
        }
175     }

177
```

```
 }

//end of loop over events (for(ii))
  double pi = 3.1415;
  double x[2000];
  double y1[2000];
  double y[2000];
  for(int i =1; i<2000;i++){
    x[i] = 0.02*i;    y1[i] = ipow(180,4)*log ((ipow(180,2)-x[i]*x[i])/
        x[i]) -0.5*x[i]*x[i]*x[i]*x[i]*log ((ipow(180,2)-x[i]*x[i])/x[i
        ]*x[i])-x[i]*x[i]*ipow(180,2)*log ((2*x[i]*x[i])/ipow(180,2))+
        ipow(180,4)*log ((ipow(180,2))/(2*x[i]*x[i]))-4*ipow(180,4)-3*x
        [i]*x[i]*x[i]*x[i]+9.25*x[i]*x[i]*ipow(180,2);
    y[i] = y1[i]*(0.11/(ipow(180,3)*12*ipow(pi,2)));
    //cout<<x[i]<<endl;
  }


  TCanvas *can = new TCanvas("", "");
  histo->Sumw2();
  histo->Draw("");

  Double_t par[2];
  TF1 *g1     = new TF1("g1","gaus",(double)iMass-10,(double)iMass+10);
  TF1 *g2     = new TF1("g2","gaus",(double)iMass2-5,(double)iMass2+25)
      ;
  TF1 *total     = new TF1("total","gaus(0)+gaus(1)",(double)iMass-10,(
      double)iMass+10);
  total->SetLineColor(2);
  histo->Fit(g1,"R");
  histo->Fit(g2,"R+");
  g1->GetParameters(&par[0]);
  g2->GetParameters(&par[1]);
  total->SetParameters(par);
  histo->Fit(total,"R+");

  /*
  TFitResultPtr r = histo->Fit("pol1","S","",(double)iMass-60,(double)
      iMass+60);
  TMatrixDSym cov = r->GetCovarianceMatrix();  //  to access the
      covariance matrix
  Double_t chi2   = r->Chi2(); // to retrieve the fit chi2
  Double_t par1   = r->Parameter(1); // retrieve the value for the
      parameter 0
  Double_t err0   = r->ParError(0); // retrieve the error for the
      parameter 0
  r->Print("V");     // print full information of fit including
      covariance matrix
  r->Write("plots.root");         // store the result in a file
```

```
    cout << "Maksimum: " << par1 << endl;
217 */

219

    histo->GetXaxis()->SetTitle("Jet invariant mass[GeV]");
221 histo->GetYaxis()->SetTitle("Number of events/10 GeV");
    histo->SetStats(0);
223 can->SaveAs("plot2.png");
    histo->Print("plot2.png");
225 f->Write("histo");

227 delete can;
    delete histo;
229



231
    TCanvas *can3 = new TCanvas("plot", "");
233 histo3->Draw("E0");
    can3->SaveAs("plot3.eps");
235 delete can3;
    delete histo3;
237
    TCanvas *can2 = new TCanvas("plot", "");
239 histo2->Draw("E0");
    can2->SaveAs("plot3.eps");
241


243 TGraph *gr3 = new TGraph (2000, x, y);
    TCanvas *c2 = new TCanvas("c2","",200,100,600,400);
245
    gr3->SetLineColor(4);
247 gr3->SetTitle("");
    gr3->GetXaxis()->SetTitle("Cut in invariant mass [GeV]");
249 gr3->GetYaxis()->SetTitle("Width [GeV]");
    gr3->Draw("AL");
251 c2->SaveAs("plot5.png");


253



255 /*
    ofstream myfile ("Info4.txt",ios::app );
257   if (myfile.is_open())
      {
259     myfile<<r->Parameter(0)<< " "<<par1<<" " << r->Parameter(2)<<"
          "<<objects[5][14]<<endl;


261



263   }
```

```
   */
265


267
   f->Close();
269
}//end of void analysis()
```

/mn/felt/u8/haavass/col/AnalysisCode/ratt.cpp

C.0.3 Code for performing the $\Delta\chi^2$ procedure

This program reads in information about the fit and the data point, performrs the statistical analysis and plots the color plot of the scaling factor.

```
1  // This program is based on an example from the ROOT tutorials website
   #include <iostream.h>
3  #include <TChain.h>
   #include <TFile.h>
5  #include <TTree.h>
   #include <TH1.h>
7  #include <TH2.h>
   #include <TGraph.h>
9  #include <TGraph2D.h>
   #include <TCanvas.h>
11 #include <TRandom.h>
   #include <TRandom3.h>
13 #include <TLorentzVector.h>
   #include "TopHist.h"
15 //A few standard headers
   #include <fstream>
17 #include <utility>
   #include <cmath>
19 #include <time.h>
   #include <vector>
21 #include "TFitResult.h"
   #include "TF1.h"
23 #include <cstdlib>
   #include <stdio.h>
25 #include <TROOT.h>
   #include <TMinuit.h>
27


29 const int iNum = 255;
   const int iNum2 = 59;
31 Float_t z[59],x1[196],x2[196],errorz[59];
   Float_t p0[196],p1[196],p2[196],cross[196],Pro[196];
33 Float_t P0[196],P1[196],P2[196],mass[59];
```

```
35 // this is the function used for the fit
   //   par: vector with the fit parameters
37 Double_t fit_function(float mass,float p0,float p1,float p2,float
       cross,float P0,float P1,float P2,float Pro,Double_t *par)
   {
39   double value=exp(5.6-0.00667*mass)+cross*Pro*0.0702*1.75*par[0]*(p0*
         exp(-0.5*(pow((mass-p1),2)/pow(p2,2)))+P0*exp(-0.5*(pow((mass-P1)
         ,2)/pow(P2,2))));
     return value;
41 }


43


45 Double_t fitfunc(float mass,float p0,float p1,float p2,float cross,
       float P0,float P1,float P2,float Pro,float n)
   {
47   double value=exp(5.6-0.00667*mass)+(p0*0.0702*1.75*cross*Pro*n*exp
         (-0.5*(pow((mass-p1),2)/pow(p2,2)))+P0*Pro*0.0702*1.75*cross*n*
         exp(-0.5*(pow((mass-P1),2)/pow(P2,2))));
    return value;
49 }


51


53


55 static int kj;


57


59
   void calc_chi_square(Int_t &npar, Double_t *gin, Double_t &f, Double_t
       *par, Int_t iflag)
61 {
     double chisq = 0;
63   for (int i=0;i<iNum2; i++) {
       // chi square is the quadratic sum of the distance from the point
           to the function weighted by its error
65     double delta  = (z[i]-(fit_function(mass[i],p0[kj],p1[kj],p2[kj],
           cross[kj],P0[kj],P1[kj],P2[kj],Pro[kj],par)))/errorz[i];
       chisq += delta*delta;
67   }
     f = chisq;
69   return;
   }
71


73 double chisquare(float q0,float q1,float q2,float CROSS,float Q0,float
```

```
    Q1, float Q2, float PRO, float N)
{
  double chisq = 0;
  for (int i=0;i<iNum2; i++) {
    // chi square is the quadratic sum of the distance from the point
       to the function weighted by its error
    double delta = (z[i]-(fitfunc(mass[i],q0,q1,q2,CROSS,Q0,Q1,Q2,PRO
       ,N)))/errorz[i];
    chisq += delta*delta;
  }
  return chisq;
}



main()
{



 vector<vector<float> > P;
  P=vector<vector<float> >(10,vector<float>(255,0));
  for(int i =0;i<255;i++){
    for (int j=0;j<10;j++){
      scanf("%e",&P[j][i]);
      //cout<<P[1][i]<<endl;
    }
  }



 for(int k =0;k<59;k++){
       mass[k] = P[0][k+196];
       z[k] = P[1][k+196];
       errorz[k] = P[2][k+196];
       //cout<<errorz[k]<<endl;
 }

for(int k =0;k<196;k++){
       x1[k] = P[0][k];
       x2[k] = P[1][k];
       p0[k] = P[2][k];
       p1[k] = P[3][k];
       p2[k] = P[4][k];
       P0[k] = P[5][k];
       P1[k] = P[6][k];
       P2[k] = P[7][k];
```

```
        cross[k] = P[8][k];
        Pro[k] = P[9][k];
        //cout<<"P0"<<P0[k]<<endl;
        //cout<<"p0 "<<p0[k]<<endl;
        if(x1[k]==x2[k]){
   P0[k] = 0.5*P0[k];
   p0[k] = 0.5*p0[k];
        }

 }


   Double_t Vec[196];
   Double_t Cro[196];
   Double_t Mass[196];
   Double_t MASS[196];


for(kj =0;kj<196;kj++){

   TMinuit *ptMinuit = new TMinuit(59);  //initialize TMinuit with a
       maximum of 59 params
   //
   //  select verbose level:
   //    default :      (58 lines in this test)
   //    -1 : minimum   ( 4 lines in this test)
   //     0 : low       (31 lines)
   //     1 : medium    (61 lines)
   //     2 : high      (89 lines)
   //     3 : maximum (199 lines in this test)
   //
   ptMinuit->SetPrintLevel();
   // set the user function that calculates chi_square (the value to
       minimize)


   ptMinuit->SetFCN(calc_chi_square);


   Double_t arglist[10];
   Int_t ierflg = 0;

   arglist[0] = 1;
   ptMinuit->mnexcm("SET ERR", arglist ,1,ierflg);

   // Set starting values and step sizes for parameters
   static Double_t vstart[1] = {1};
   static Double_t step[1] = {1};
   ptMinuit->mnparm(0, "a1", vstart[0], step[0], 0,0,ierflg);
```

```
// Now ready for minimization step
  arglist[0] = 500;
  arglist[1] = 1.;
  ptMinuit->mnexcm("MIGRAD", arglist ,1,ierflg);


  // Print results
  cout << "\nPrint results from minuit\n";
  double fParamVal;
  double fParamErr;
  ptMinuit->GetParameter(0,fParamVal,fParamErr);
  cout << "a1=" << fParamVal << "\n";


  // if you want to access to these parameters, use:
  Double_t amin,edm,errdef;
  Int_t nvpar,nparx,icstat;
  ptMinuit->mnstat(amin,edm,errdef,nvpar,nparx,icstat);



  //void mnstat(Double_t &fmin, Double_t &fedm, Double_t &errdef,
      Int_t &npari, Int_t &nparx, Int_t &istat)
  //*-*-*-*-*Returns concerning the current status of the minimization
      *-*-*-*-*
  //*-*       ==========================================================
  //*-*         User-called
  //*-*           Namely, it returns:
  //*-*          FMIN: the best function value found so far
  //*-*          FEDM: the estimated vertical distance remaining to
      minimum
  //*-*          ERRDEF: the value of UP defining parameter
      uncertainties
  //*-*          NPARI: the number of currently variable parameters
  //*-*          NPARX: the highest (external) parameter number defined
      by user
  //*-*          ISTAT: a status integer indicating how good is the
      covariance
  //*-*              matrix: 0= not calculated at all
  //*-*                      1= approximation only, not accurate
  //*-*                      2= full matrix, but forced positive-
      definite
  //*-*                      3= full accurate covariance matrix
  //
      *-*-*-*-*-*-*-*-*-*-*-*-*-*-*-*-*-*-*-*-*-*-*-*-*-*-*-*-*-*-*-*-*-*-*-*-*
```

```
/*
cout << "\n";
cout << " Minimum chi square = " << amin << "\n";
cout << " Estimated vert. distance to min. = " << edm << "\n";
cout << " Number of variable parameters = " << nvpar << "\n";
cout << " Highest number of parameters defined by user = " << nparx << "\n";
cout << " Status of covariance matrix = " << icstat << "\n";

cout << "\n";
*/
ptMinuit->mnprin(3,amin);
//*-*-*-*-Prints the values of the parameters at the time of the call *-*-*-*-*
//*-*    ==================================================================
//*-*          also prints other relevant information such as function value,
//*-*          estimated distance to minimum, parameter errors, step sizes.
//*-*
//*-*           According to the value of IKODE, the printout is:
//*-*    IKODE=INKODE= 0    only info about function value
//*-*                  1    parameter values, errors, limits
//*-*                  2    values, errors, step sizes, internal values
//*-*                  3    values, errors, step sizes, first derivs.
//*-*                  4    values, parabolic errors, MINOS errors
//*-*    when INKODE=5, MNPRIN chooses IKODE=1,2, or 3, according to ISW(2)
//*-*-*-*-*-*-*-*-*-*-*-*-*-*-*-*-*-*-*-*-*-*-*-*-*-*-*-*-*-*-*-*-*-*-*-*-*-*-*-*-*-*-*-*-*

 double Nu = fParamVal;
 double chis = amin;
 //cout<<chis<<endl;


 while((chis-amin) <=3.84 ) {
   Nu+=0.00001;
   chis = 0;
   for (int i=0;i<iNum2; i++) {
     // chi square is the quadratic sum of the distance from the point to the function weighted by its error
     double delta  = (z[i]-fitfunc(mass[i],p0[kj],p1[kj],p2[kj],cross[kj],P0[kj],P1[kj],P2[kj],Pro[kj],Nu))/errorz[i];
     chis += delta*delta;

    }
```

```
245
    }
247
    cout<<Nu<<" "<<chis-amin<<endl;
249


251


253 //cout<<"Num"<<chi-amin<<endl;


255
    Cro[kj] = cross[kj]*Pro[kj];
257 Vec[kj] = Nu;
    Mass[kj] = x2[kj];
259 MASS[kj] = x1[kj];
  }
261
  for (int i=0;i<196; i++) {
263 cout<<i<<" "<<Vec[i]<<endl;
  }
265
   Float_t N1[400];
267 Float_t C1[400];
   Float_t C2[400];
269 Float_t C3[400];

271 for (int i=0;i<400; i++) {
     N1[i] = -2+0.01*i;
273  C1[i] = chisquare(p0[74],p1[74],p2[74],cross[74],P0[74],P1[74],P2
        [74],Pro[74],N1[i]);
     C2[i] = 0.9986;
275  C3[i] = i;
   }
277


279
TCanvas *c2 = new TCanvas("c","Graph2D example",0,0,700,600);
281 Int_t np = 196;
TGraph2D *dt = new TGraph2D("dt");
283 TRandom *r = new TRandom();

285 for (Int_t N=0; N<np; N++) {
   dt->SetPoint(N,Mass[N],MASS[N],Vec[N]);
287 cout << Mass[N] << " " << MASS[N] << " " << Vec[N] << endl;
}
289 //gStyle->SetPalette(1);
 gPad->SetLogz();
291 dt->SetNpx(50);
 dt->SetNpy(50);
```

```
293  dt->GetXaxis()->SetTitle("Squark Mass [GeV]");
     dt->GetYaxis()->SetTitle("Gluino Mass [GeV]");
295  dt->SetTitle(" ");
     dt->SetMaximum(2.0);
297  dt->SetMinimum(0.002);
     dt->Draw("colz");
299  c2->SaveAs("plot3.png");

301 TFile *f = new TFile("are.root","recreate");
    f->Write("dt");
303 f->Close();


305
     c2->SaveAs("plot3.eps");
307



309
     TCanvas *c3 = new TCanvas("c3","",0,0,700,600);
311  TGraph *gr3 = new TGraph (400, N1, C1);
     TGraph *gr2 = new TGraph (400, C2, C3);
313
     gr3->SetLineColor(4);
315  // gr3->Draw("AL");
     gr3->GetXaxis()->SetTitle("n");
317  gr3->GetYaxis()->SetTitle("Chi squared");
     gr3->Draw("AL");
319  gr2->Draw("");
     gr3->SetTitle(" ");
321  c3->SaveAs("plot1.eps");


323
     return EXIT_SUCCESS;
325 //return Nu;

327 }
```

/mn/felt/u8/haavass/rootsimple/AnalysisCode/ratt.cpp

Bibliography

[1] **CMS** Collaboration, "Search for Three-Jet Resonances in pp Collisions at sqrt(s) = 7 TeV," *Phys.Rev.Lett.* **107** (2011) 101801.

[2] R. Haag, J. T. Lopuszanski, and M. Sohnius, "All Possible Generators of Supersymmetries of the S Matrix," *Nucl.Phys.* **B88** (1975) 257.

[3] S. P. Martin, "A Supersymmetry primer," `arXiv:hep-ph/9709356 [hep-ph]`.

[4] R. Barbier, C. Berat, M. Besancon, M. Chemtob, A. Deandrea, *et al.*, "R-parity violating supersymmetry," *Phys.Rept.* **420** (2005) 1–202, `arXiv:hep-ph/0406039 [hep-ph]`.

[5] S. Coleman and J. Mandula, "All Possible Symmetries of the S Matrix," *Phys. Rev.* **159** (Jul, 1967) 1251–1256.

[6] Harald J.W. Müller-Kirsten and Armin Wiedemann, *Introduction to Supersymmetry*. World Scientific Publishing Co. Pte. Ldt., second ed., 2010.

[7] J. Bagger and J. Wess, "Partial Breaking of Extended Supersymmetry," *Phys.Lett.* **B138** (1984) 105.

[8] **LEP Higgs Working Group for Higgs boson searches, OPAL, ALEPH, DELPHI, L3** Collaboration, "Search for the Standard Model Higgs boson at LEP," `arXiv:hep-ex/0107029 [hep-ex]`. The Results quoted in this paper are not final.

[9] **ATLAS** Collaboration, G. Aad *et al.*, "Search for the Standard Model Higgs boson in the diphoton decay channel with 4.9 fb^{-1} of pp collisions at sqrt(s)=7 TeV with ATLAS," *Phys.Rev.Lett.* **108** (2012) 111803, `arXiv:1202.1414 [hep-ex]`.

[10] **CMS** Collaboration, S. Chatrchyan *et al.*, "Combined results of searches for the standard model Higgs boson in pp collisions at sqrt(s) = 7 TeV," `arXiv:1202.1488 [hep-ex]`.

[11] **ATLAS** Collaboration, G. Aad *et al.*, "Search for squarks and gluinos using final states with jets and missing transverse momentum with the ATLAS detector in sqrt(s) = 7 TeV proton-proton collisions," *Phys.Lett.* **B710** (2012) 67–85, arXiv:1109.6572 [hep-ex].

[12] F. Zwicky, "Spectral displacement of extra galactic nebulae," *Helv.Phys.Acta* **6** (1933) 110–127.

[13] V. C. Rubin and J. Ford, W. Kent, "Rotation of the Andromeda Nebula from a Spectroscopic Survey of Emission Regions," *Astrophys.J.* **159** (1970) 379–403.

[14] **Super-Kamiokande** Collaboration, H. e. a. Nishino, "Search for proton decay via $p \to e^+\pi^0$ and $p \to \mu^+\pi^0$ in a large water cherenkov detector," *Phys. Rev. Lett.* **102** (Apr, 2009) 141801.

[15] **Particle Data Group** Collaboration, K. Nakamura *et al.*, "Review of particle physics," *J.Phys.G* **G37** (2010) 075021.

[16] M. Cacciari, G. P. Salam, and G. Soyez, "The anti-k_t jet clustering algorithm," *JHEP* **0804** (2008) 063.

[17] M. Bahr, S. Gieseke, M. Gigg, D. Grellscheid, K. Hamilton, *et al.*, "Herwig++ Physics and Manual," *Eur.Phys.J.* **C58** (2008) 639–707, arXiv:0803.0883 [hep-ph].

[18] M. Cacciari, G. P. Salam, and G. Soyez, "FastJet user manual," *Eur.Phys.J.* **C72** (2012) 1896, arXiv:1111.6097 [hep-ph].

[19] B. Allanach, C. Balazs, G. Belanger, M. Bernhardt, F. Boudjema, *et al.*, "SUSY Les Houches Accord 2," *Comput.Phys.Commun.* **180** (2009) 8–25, arXiv:0801.0045 [hep-ph].

[20] W. Beenakker, R. Hopker, and M. Spira, "PROSPINO: A Program for the production of supersymmetric particles in next-to-leading order QCD," arXiv:hep-ph/9611232 [hep-ph].

[21] F. James, "MINUIT - Function Minimization and Error Analysis - Reference Manual," 2000. http://wwwasdoc.web.cern.ch/wwwasdoc/minuit/minmain.html.

[22] T. Sjostrand, S. Mrenna, and P. Z. Skands, "PYTHIA 6.4 Physics and Manual," *JHEP* **0605** (2006) 026, arXiv:hep-ph/0603175 [hep-ph].

[23] R. Horsky, M. Kramer, A. Muck, and P. M. Zerwas, "Squark Cascade Decays to Charginos/Neutralinos: Gluon Radiation," *Phys.Rev.* **D78** (2008) 035004, `arXiv:0803.2603 [hep-ph]`.

[24] I. Antcheva, M. Ballintijn, B. Bellenot, M. Biskup, R. Brun, *et al.*, "ROOT: A C++ framework for petabyte data storage, statistical analysis and visualization," *Comput.Phys.Commun.* **182** (2011) 1384–1385.